

NRL Report 5549

WIND-INDUCED TORQUES MEASURED ON A LARGE ANTENNA

James W. Titus

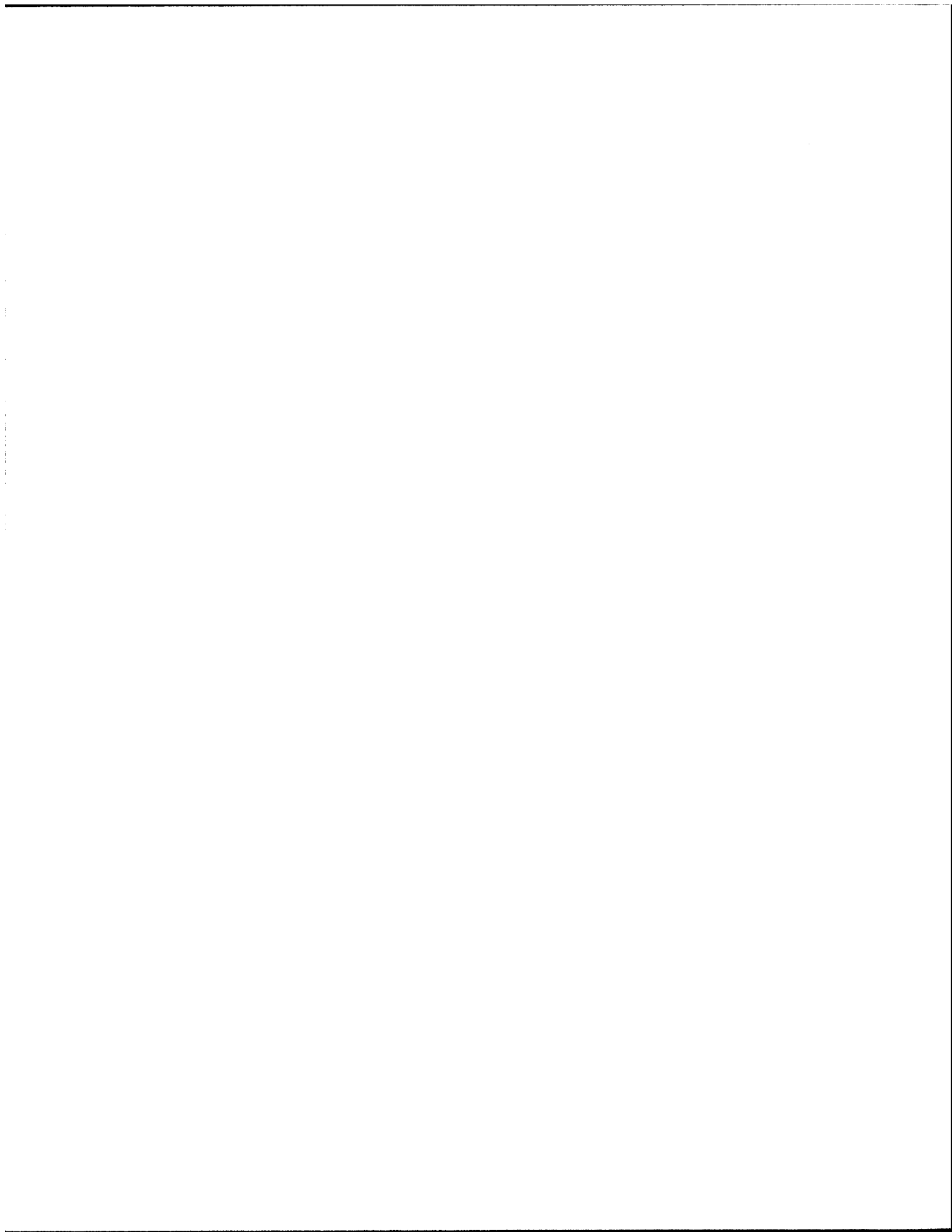
Equipment Research Branch
Radar Division

December 27, 1960



**APPROVED FOR PUBLIC
RELEASE • DISTRIBUTION
UNLIMITED**

U. S. NAVAL RESEARCH LABORATORY
Washington, D.C.



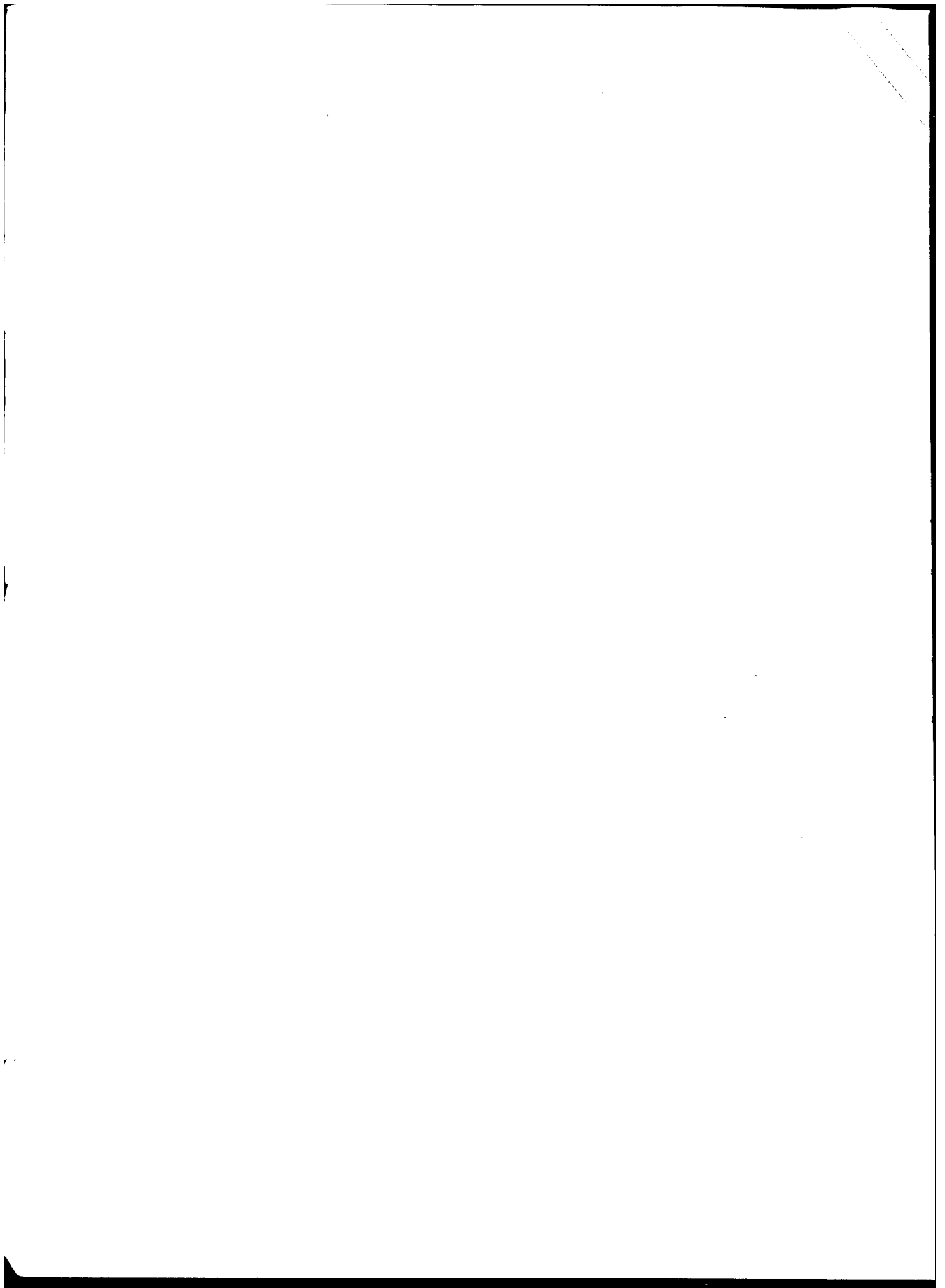
1. TASK LONG TITLE Measurement of Wind-Induced Torques in Large Antennas		2. TASK NO.
1.A. SHORT TITLE (26 spaces only) Wind Torques		3. SECURITY OF TASK
5. REPORT TYPE A. <input type="checkbox"/> INITIAL <input type="checkbox"/> REVISED CONTENT <input type="checkbox"/> ANNUAL PROGRESS <input checked="" type="checkbox"/> TERMINATION		4. DATE
B. <input checked="" type="checkbox"/> BASIC RESEARCH <input type="checkbox"/> APPLIED RESEARCH <input type="checkbox"/> DEVELOPMENT <input type="checkbox"/> T&E		6. TECHNICAL SUB-AREA
8. CONTRACTOR OR LABORATORY U. S. Naval Research Laboratory Washington 25, D. C.		7. TASK OFFICE
9. CONTRACT OR WORK ORDER 53R07-12	10. PRINCIPAL INVESTIGATOR Peter Vaternano	
11. TASK DURATION PERIOD: FROM (Date) April 1957 TO (Date) 31 June 1961		
12. ESTIMATED ANNUAL SUPPORT LEVEL <input type="checkbox"/> UNDER \$25,000 <input type="checkbox"/> \$25,000-50,000 <input type="checkbox"/> \$50,000-100,000 <input type="checkbox"/> \$100,000-500,000 <input type="checkbox"/> \$500,000-1,000,000 <input type="checkbox"/> OVER \$1,000,000		

13. WORK DESCRIPTION (List significant accomplishments upon completion or termination.)

The aim of these studies is to measure the fluctuating torques produced by wind forces impinging upon large radar antennas for purposes of evaluating the effect upon the servo drive system, as well as providing mechanical design data. Measurements made upon a 6-foot parabolic antenna, the analysis of the data obtained, and the results of analysis were published in an NRL Report. Additional wind torque measurements about both train and elevation axes will be made on other large antennas if funds are available.

14. REPORTS DISTRIBUTED (Give author, title, and appropriate report identification no.)

NRL Report 5549, "Wind Induced Torques Measured on a Large Antenna," James W. Titus, 27 Dec 1960.



CONTENTS

Abstract	ii
Problem Status	ii
Authorization	ii
INTRODUCTION	1
DESCRIPTION OF ANTENNA AND SITE	3
INSTRUMENTATION FOR MEASUREMENT	7
Introduction	7
Strain Instrumentation	7
Preload Mechanism	10
Wind Instrumentation	10
Recording	10
Calibration	11
Performance of Torque Instrumentation	11
FIELD PROCEDURE	13
ANALYSIS	15
Spectrum Analysis of Recordings	15
Other Analysis	18
RESULTS	21
Relations Between Spectral-Density Characteristics and Wind Velocity	21
Moment Coefficients	31
Root-Mean-Square Torque Data	33
Limitations of Results	36
Application of Results	37
CONCLUSIONS	38
ACKNOWLEDGMENTS	39
APPENDIX A - Analysis of Strain Amplification System	40
APPENDIX B - Values of First Corner Frequency	45

ABSTRACT

The fluctuating torques applied by wind forces are an important source of error in the servo systems required to aim large antennas for radar and radio astronomy. As a step toward providing design information for estimating and minimizing these errors, direct measurements were made of the wind-induced torque acting about the elevation axis of a 60-ft Kennedy paraboloidal antenna. Torque was measured by a strain-gage bridge and recorded on magnetic tape. Sixty runs, each of 33 minutes duration, were recorded. A mean-squared torque spectral-density curve was obtained for each run. A two-variable function of the form used by Newton and others gives a good fit with these data. The half-power frequency values ranged from 0.029 to 0.29 radian per second, with a median value of 0.11 radian per second. A second corner frequency in the vicinity of 2.0 radians per second was also observed.

Peak torques were observed during certain runs, and equivalent aerodynamic moment coefficients were derived. Root-mean-square values of wind-torque variation were obtained for all runs.

PROBLEM STATUS

This is an interim report on one phase of the problem; work on this and other phases is continuing.

AUTHORIZATION

NRL Problem R05-04
Project RF 008-04-41-4500

Manuscript submitted July 29, 1960.

WIND-INDUCED TORQUES MEASURED ON A LARGE ANTENNA

INTRODUCTION

In the design of the servo systems which are required to aim tracking antennas for radar and radio astronomy, a number of performance requirements must be met. The basic requirement, and the one which receives most attention in the literature, is the tracking problem, which is determined by the path of the intended targets and by the allowable error. This report is concerned with another major problem—that created by “output disturbances” such as wind and ice loads acting on the surfaces and structure. In the case of large parabolic antennas, the fluctuating torques applied by wind forces require serious consideration as a design factor, especially for equipments required to operate in adverse weather conditions. When tracking rates and accelerations are small, as in most radio-astronomical applications, the wind-induced disturbances may become the limiting design factor even when the winds are moderate.

Needless to say, the use of a radome eliminates this design problem. However, radomes have their own problems, and because of their great cost and their possible effect upon the antenna pattern, they may not offer the best solution in all cases. The need, therefore, will continue for the designers of many large antennas to consider analytically the effect of wind-induced torque upon the pointing accuracy of an antenna.

If wind velocity could be represented as a constant or as a slowly changing quantity, a fairly straightforward application of aerodynamic drag coefficients would give a torque value for any desired combination of antenna position and wind velocity. This procedure is, of course, useful for structural design, and it has even been used with some success to predict the power requirements for a constant-velocity azimuth drive on a search radar antenna.* Unfortunately, the outstanding characteristic of wind velocity measured at low altitudes over shore sites is its random variation, both in magnitude and in direction. As an example of this variation, Fig. 1 shows simultaneous recordings of wind speed and direction measured at one antenna site over a period of several minutes.

Analytical methods have been developed for determining the mean-square error caused in a system by the application of a stochastic disturbance, and further, for minimizing this error.† These methods require a statistical description of the disturbance, in the form of an autocorrelation function or of a power density spectrum ($1/2\pi$ times the Fourier transform of the autocorrelation function). Since the disturbance of interest to this study is a torque, the transformed function may be more meaningfully described as the “mean-squared torque spectral density” (in this report, the term “torque spectral density” will be used for brevity). One procedure for deriving this function would begin by using an antenna “aerodynamic constant” to operate upon an expression representing the characteristics of the wind. Neglecting the effect of velocity changes upon drag coefficients, as well as the effects

* P. A. Crosby and D. A. Regillo, “Rotative Power for Large Antennas,” Am. Soc. Mech. Engrs. Paper No. 59-A-268.

† J. G. Truxal, “Automatic Feedback Control System Synthesis,” Ch. 8, New York:McGraw-Hill, 1955.
G. C. Newton, L. A. Gould, and J. F. Kaiser, “Analytical Design of Linear Feedback Controls,” New York:Wiley, 1957.

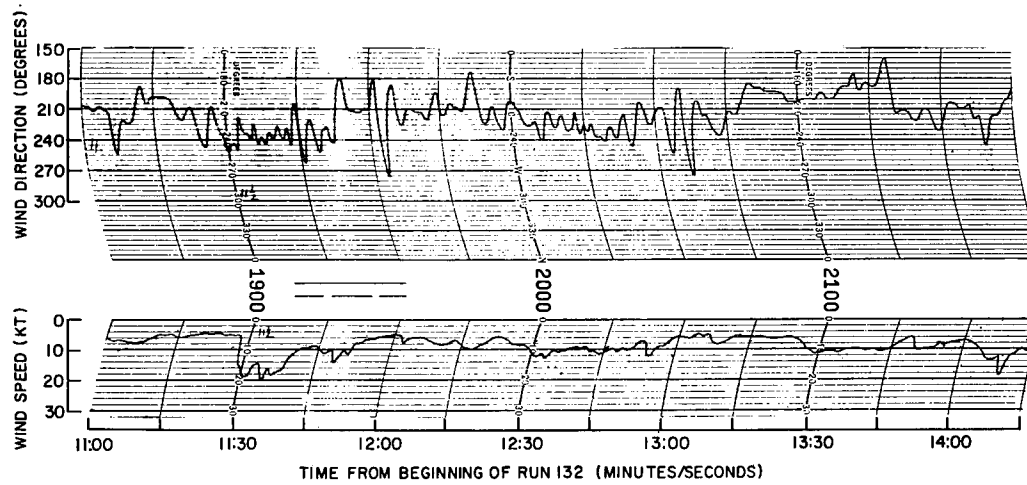


Fig. 1 - Wind at NRL antenna site, Stump Neck Annex, April 8, 1959

of fluctuation in wind direction, and further assuming that the variations in velocity are relatively small, the variation in wind torque can be expressed by the following:

$$M_f = 2K_w \bar{V} V(t) \quad (1)$$

where M_f = fluctuation in wind torque, lb ft

K_w = antenna aerodynamic constant, lb ft per (ft/sec)²

\bar{V} = mean wind velocity, ft/sec

$V(t)$ = instantaneous variation of wind velocity from its mean value, ft/sec.

Given a suitable statistical description of the wind-velocity fluctuation $V(t)$ and Eq. (1), a torque density spectrum can be obtained and used analytically to predict servo-system error. While this approach is undoubtedly adequate for antennas of the order of 10 feet in diameter, it is difficult at this time to justify its use for large antennas, if their tracking requirements are at all exacting. Among the problems relating particularly to this approach may be listed the following:

1. Can wind data taken at a single point be used as a tolerable substitute for the complex structure of actual wind?
2. If not, how detailed must on-site data be, in order to describe the wind adequately?
3. Over how long a period of time need these data be collected?
4. How is an accurate "aerodynamic constant" to be obtained, and how good is it?
5. To how great an extent does the presence of the antenna structure invalidate the use of on-site wind data taken before its construction?

A direct measurement of the fluctuating wind torque made upon an existing antenna evidently bypasses these problems, except for the question of time, and should yield a sound basis from which a statistical expression of the torque may be derived. The expression could then be used in design or analysis of the servo system in which this particular

antenna is the major component. It is believed that in the absence of better data (the present situation), the results of such measurements could be useful in the design of control systems for other antennas.

This report describes the measurements of wind-induced elevation-axis torque made by members of the Equipment Research Branch, Radar Division, upon a 60-ft-diameter parabolic antenna. Results are presented and discussed.

The elevation-axis torque was obtained by calibrating and measuring the strain in the crank arm which moves the antenna about the elevation axis. The output of a strain-gage bridge was recorded on magnetic tape. Sixty runs, each of 33 minutes duration, were recorded on 19 different days during the months of October, 1958, and February through June, 1959. Runs were made with the antenna at three different elevation angles and five different azimuth angles relative to the wind.

Mean-squared torque spectral density curves were obtained for the time interval represented by each run, with the aid of a spectrum analyzer. It was found that these curves could be approximated by the equation

$$\Phi_{TT} = K \left(\frac{\omega_0^2}{\omega_0^2 + \omega^2} \right) \left(\frac{\omega_1^2}{\omega_1^2 + \omega^2} \right). \quad (2)$$

In this equation, ω is the frequency variable, ω_0 is the half-power frequency, or "first corner frequency," and ω_1 the "second corner frequency." The low-frequency value K of the function was found to be a fourth-power variable of the average wind velocity, while ω_0 varies slightly around a mean value of 0.12 rad/sec. The quantity ω_1 , evaluated for only three runs, ranged between 1.6 and 2.4 rad/sec.

Peak torques were observed during certain runs, and equivalent aerodynamic moment coefficients were derived. Root-mean-square values of wind torque variation were obtained for all runs.

DESCRIPTION OF ANTENNA AND SITE

The measurements to be described were taken upon a 60-ft-diameter, azimuth-elevation mounted paraboloidal antenna located at a field station of NRL. The antenna, shown in Fig. 2, was built in 1956 by the D. S. Kennedy Company of Cohasset, Mass. The paraboloidal surface, 60 feet in diameter, is made of 3/8 x 0.064 in. "Squarex" expanded aluminum metal on a framework of aluminum tubing. A truss, also of aluminum tubing, serves to attach this paraboloid to the ends of the elevation shaft of an azimuth-elevation mount. The antenna feed is supported at the focal point by three laminated fiberglass spars.

The mount, which serves to support and to aim the paraboloid, consists principally of a base, an azimuth turntable with drive mechanism, an elevation shaft with drive unit, and the data readout systems. The steel base structure (Fig. 2) is bolted to the top of a two-storey concrete blockhouse, about 20 ft high. The azimuth turntable, at the top of the cylindrical portion of the base, is driven by an electric motor acting through a gear drive inside the base. This turntable carries the elevation shaft bearings and the elevation drive unit. The elevation shaft to which attaches the truss which supports the paraboloid is rotated about its axis by a ball-bearing jackscrew acting on the elevation crank arm, as sketched in Fig. 3. (Part of this mechanism can be seen in Fig. 4.) The jackscrew, in turn, is driven by an electric motor acting through a gear train inside the elevation drive housing. The altitude of the elevation axis is approximately 57 ft above the nearby ground.



Fig. 2 - NRL 60-ft antenna

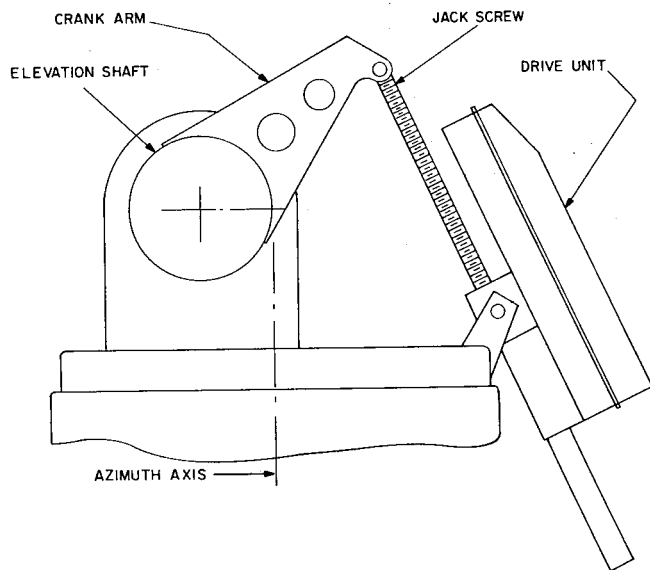


Fig. 3 - Elevation-drive mechanism

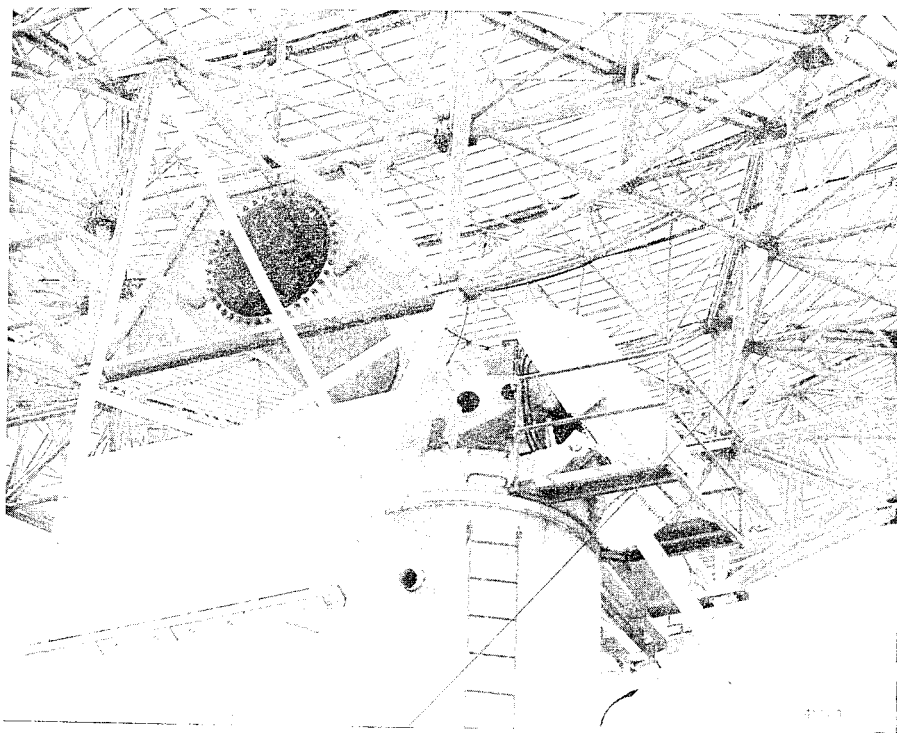


Fig. 4 - Closeup view of antenna, showing elevating mechanism

The juncture of the paraboloid supporting truss with the left-hand end of the elevation shaft, part of the left-hand elevation bearing housing, part of the crank arm, the elevation drive housing, and the elevation drive jackscrew pivot bearing can be seen in Fig. 4.

The antenna site, a small clearing in a densely wooded area, is located at the high point (elevation approximately 140 ft) of a small plateau in the eastern part of the Stump Neck Annex of the Indian Head Naval Powder Factory.* Seven hundred yards to the north, an 80-ft bluff overlooks the mile-wide mouth of the Mattawoman Creek, and the Potomac River. Another steep drop, a thousand yards to the west, overlooks a marsh, the low-lying land of Stump Neck, and the river beyond. To the south, the land drops gradually from the site to the course of a branch 400 yards distant and 70 ft below the site elevation. The land to the east is nearly level for a distance of 800 yards. Beyond this it is broken by a succession of steep-walled ravines. With the exception of two roads to the north, and a clearing of about two acres northwest of the site, the land is wooded to a radius of 800 yards or more in all directions from the site.

The plan view, Fig. 5, shows the locations of the blockhouse, service tower, and access road, and the outline of the cleared area. Beyond the limits of this cleared area, trees have been cut so that none are higher than about 56 ft above the ground in this area. An aerial photograph of the site is shown in Fig. 6.

* Indian Head, Md, Va Sheet 5561 II SW, Series V833, Army Map Service.

NAVAL RESEARCH LABORATORY

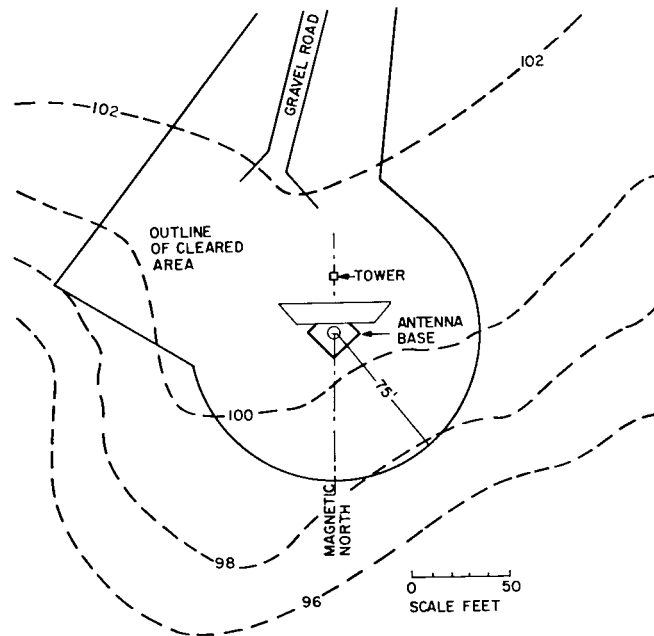


Fig. 5 - Plan of antenna site

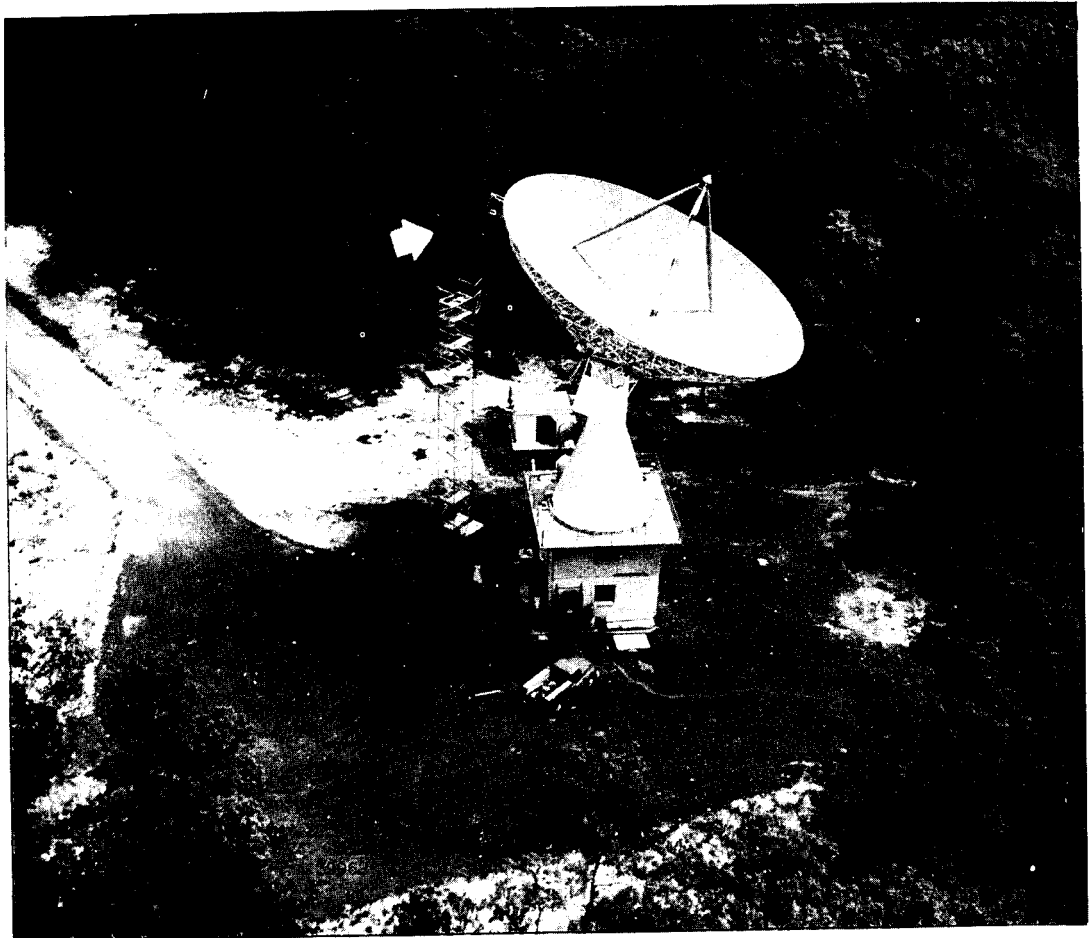


Fig. 6 - Aircraft view of antenna site

INSTRUMENTATION FOR MEASUREMENT

Introduction

Initially, it was desired that instrumentation be provided which would give a continuous indication of torque exerted on the antenna by winds from 5 to 50 knots. Since the measurements were to be made only during intervals between periods of antenna use, it was necessary that the installation neither interfere with nor be damaged by operation of the antenna. The frequency range expected to be of greatest interest for design of control systems was that from 0.1 to 10.0 radians per second. No exact specification was placed on accuracy; the initial objective was merely to produce information which would have sufficient accuracy to be significant.

Three general methods of measuring antenna torque which immediately suggest themselves are:

1. Use of external equipment to restrain the antenna and measure torque
2. Use of a drive motor as a dynamometer
3. Measuring strain in one of the structural members which are loaded by an applied torque.

The large size of the antenna precluded serious consideration of external torque measuring equipment. The dynamometer approach was discarded because the uncertain transmission characteristic of the elevation drive system, and especially of the jack screw, would have made any measurements about the elevation axis most difficult, if not impossible, to interpret. The large magnitudes of the coulomb friction and the lost motion in the azimuth drive similarly appeared to preclude dynamometer measurement of azimuth torques.

The use of strain measurements was much more promising. It appeared, for example, that measurement of the bending in the elevation crank arm (Fig. 3) would provide good information on elevation torque. Measurement of torsion in the antenna base would give a description of the azimuth torque. It was decided initially to make measurements about the elevation axis only, in order to limit the magnitude of work undertaken.

Strain Instrumentation

In order to obtain frequency spectra of the wind torque, it was first necessary to measure and record this torque as a time function. A block diagram of the instrumentation appears as Fig. 7. Any torque applied to the paraboloid will be applied in turn to the elevation crank arm, causing a deflection of this arm approximately proportional to the applied torque. This deflection is sensed by a strain-gage bridge supplied with a 19.5-cps reference voltage. The output of the strain-gage bridge is amplified, and is then recorded by a magnetic-tape recorder.

The desire to conduct measurements in winds of from 5 to 50 knots was interpreted for design purposes as a requirement to measure torques from 1500 to 200,000 lb ft. Approximate calculations indicated that for the lower torque value, the stress in the extreme fibres of the steel elevation crank arm would be of the order of 40 lb/in.². Members of the Mechanics Division had advised that SR-4 strain gages would give inaccurate results at the low strains corresponding to this stress (1.4×10^{-6} in./in.), especially when the strain would reverse from tension to compression.

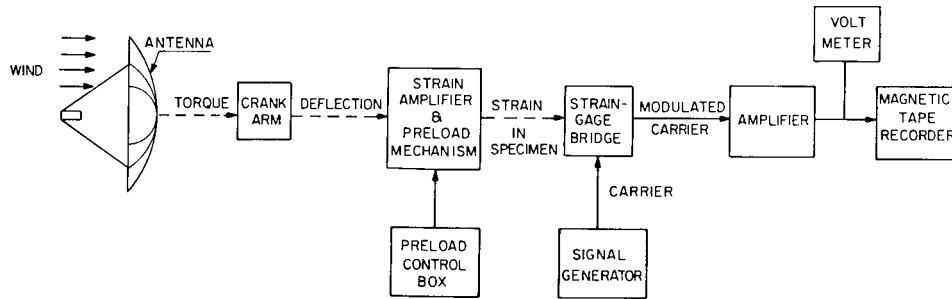


Fig. 7 - Block diagram of instrumentation

The difficulty of working with small strains subject to reversal was overcome to a large degree by the use of a "strain multiplier" and preload mechanism. The principle of strain multiplication used may be explained simply by applying ordinary engineering analysis to a cantilever beam of constant cross section. The beam of length L_1 shown in Fig. 8a is subjected to a concentrated load P . Let

E = modulus of elasticity of the beam

I = moment of inertia of the cross section of the beam

c = distance from the neutral axis of the beam to the extreme fiber

$M_1 = PL_1$ = maximum bending moment.

The corresponding maximum normal strain is given by

$$\epsilon_1 = \frac{M_1 c}{EI} = \frac{PL_1 c}{EI} \quad (3)$$

Let δ be deflection at the end of the beam. Then

$$\delta = \frac{PL_1^3}{3EI} \quad (4)$$

Now suppose that a point of the fixed structure is available near the end of the beam so that a tension member can be connected from the end of the beam to the fixed structure, as indicated in Fig. 8b. This member, designated Part 2 in the figure, will be called the "strain specimen" in this report. If this strain specimen has negligible axial stiffness, it will not affect the value of δ . Furthermore, since it is attached to the end of the beam, the total deflection of the specimen will also be equal to δ .

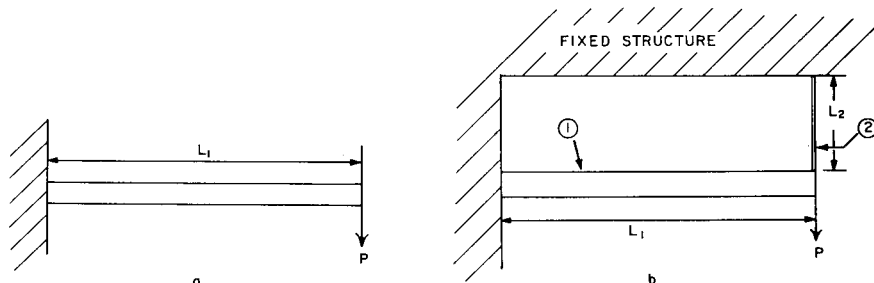


Fig. 8 - Principle of strain measurement

Let ϵ_2 be the normal strain in the specimen. Then

$$\epsilon_2 = \frac{\delta}{L_2} \quad (5)$$

where L_2 is the length of the specimen (assuming uniform cross section). Substituting for δ from Eq. (4),

$$\epsilon_2 = \frac{PL_1^3}{3EIL_2} \quad (6)$$

The ratio of the strain in the specimen to the maximum strain in the beam is then

$$\frac{\epsilon_2}{\epsilon_1} = \frac{L_1^2}{3cL_2} \quad (7)$$

This equation, then, expresses the strain multiplication, or "amplification" which would be obtained if the specimen could be made of negligible stiffness compared to the beam. As an example, assume the length of the beam to be 30 in., the length of the strain specimen 2 in., and the depth of the beam 10 in. ($c = 5$ in.). Then

$$\frac{\epsilon_2}{\epsilon_1} = \frac{30^2}{3 \times 5 \times 2} = 30.$$

The strain-measuring equipment is shown in Fig. 9 as mounted in the laboratory for test. In this setup, the larger steel beam at the bottom, Part 1, is used to simulate the member whose strain is to be measured, i.e., the elevation crank arm. The upper beam (a 6-in. H-beam) performs the function of the fixed member of Fig. 8. The tensile strain specimen, shown as Part 2, is made of magnesium with a cross-sectional area of only 0.0178 sq in., so that its stiffness will be small compared with that of the beams. The design of these members is more fully explained in Appendix A. The strain specimen is shown in Fig. 10 with strain gages attached.

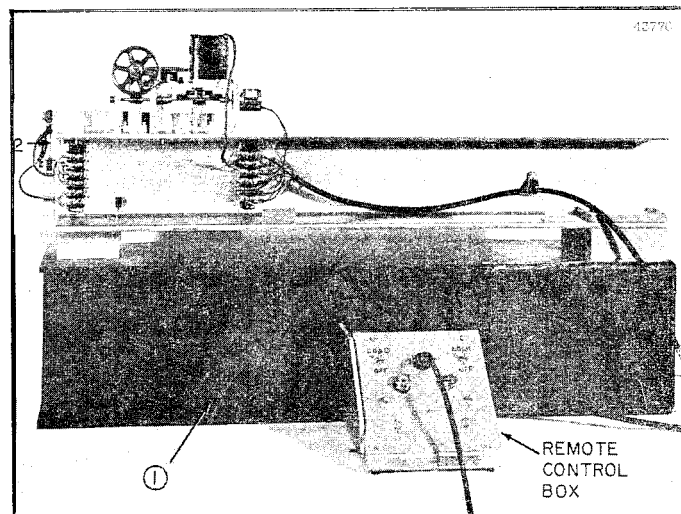


Fig. 9 - Strain-measuring equipment setup in laboratory

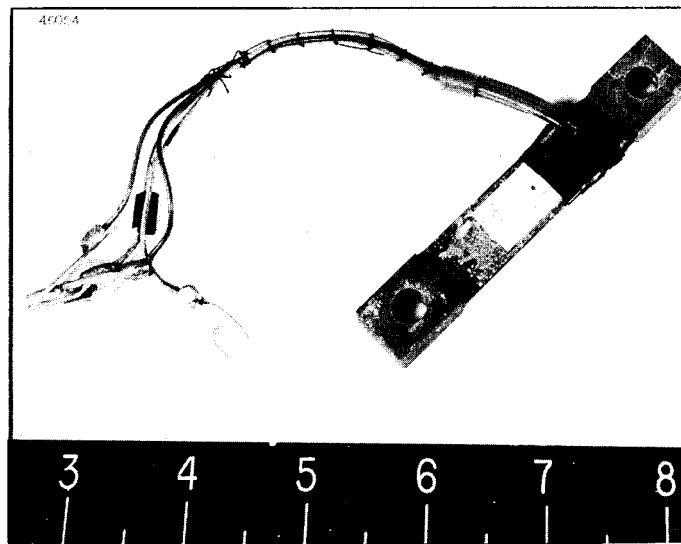


Fig. 10 - Strain specimen

Preload Mechanism

Since the strain specimen is usable only when under tension, a device was required to adjust and maintain a tensile preload on the member. A remotely controlled preloading mechanism was designed for this purpose. The mechanism, mounted on the H-beam, is shown as set up in the laboratory in Fig. 11. The specimen is clamped to one end of a lever. A lead screw operated by a size 15 two-phase motor through a 10,000:1 gear reduction presses upon the lever on the opposite side of the fulcrum to apply tension to the specimen. Another lead screw, driven by a 1-rpm gear motor, drives a traveling nut which locks the mechanism after adjustment. At full speed, the tensile strain in the specimen is increased at the average rate of approximately 26 microinches per second. The remote-control unit for the two motors is shown in the lower part of Fig. 9. An important secondary function of the preload mechanism is the adjustment of the carrier level of the input to the recorder.

Wind Instrumentation

The objective of the wind instrumentation was originally intended merely to characterize the type of wind blowing during a run. Wind velocity and direction were measured, transmitted, and indicated by the Wind Measuring Set AN/UMQ-5. The aerovane-type transmitter was mounted at an elevation of 70 ft above the ground on a mast extending above the servicing platform north of the antenna. This aerovane can be seen in Fig. 6. The velocity and direction signals were recorded by a Wind Recorder NAX-1-48 (pen and ink). The calibration of this wind measuring set was checked by mounting it above a rail car and running at various constant speeds over a section of the Washington, Brandywine, and Point Lookout Railroad.

Recording

The output of the strain-gage bridge was amplified and recorded by an Ampex Recorder, Model 401 A, using Mylar tape. The tape drive of the recorder had previously been

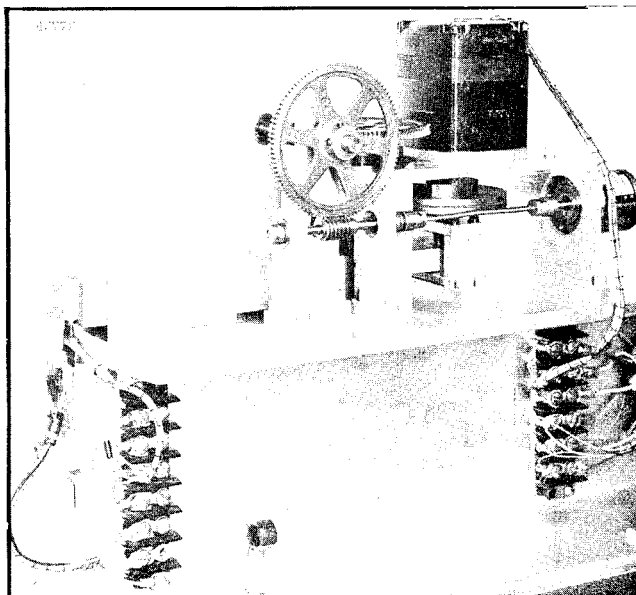


Fig. 11 - Preload mechanism and strain specimen

modified at NRL to provide extremely low tape speeds. Choice of tape speed is discussed below in the section on "Spectrum Analysis." A carrier frequency of 19.5 cps was chosen to avoid interference problems.

Calibration

The initial calibration of the torque-measuring instrumentation was obtained as follows. The strain-gage bridge was balanced with no load, and 2 volts excitation. A preload was then applied to obtain a predetermined voltage level at the bridge output. Calibration was then obtained by applying a known torque to the antenna and observing the amplified output of the strain-gage bridge as indicated by the voltmeter (Fig. 7). Torque was applied with the antenna in the stowed (90-degree elevation) position by exerting a downward force on a line attached to the framework of the antenna at an effective radius of 10 ft. The force was measured with a spring scale. A calibration curve of bridge voltage versus torque is presented on Fig. 12.

When the antenna is pointed at the zenith, with the elevation crank arm horizontal, a small weight placed on the H-beam supporting the upper end of the strain-gage "specimen" produces the same strain in the specimen as a large torque applied directly to the antenna. The factor relating the strains produced by the two procedures was obtained by performing this secondary calibration immediately after the direct procedure. Subsequent calibrations using the small weight were made frequently during the life of the project to guard against shift of amplifier gain, change in gage sensitivity, or other factors.

Performance of Torque Instrumentation

Dynamic Range - The strain instrumentation shown on the block diagram of Fig. 7 and described above proved sufficiently sensitive to give indications whenever the wind velocity reached 1 knot. The only upper limit on torques to be measured would be the failure of the

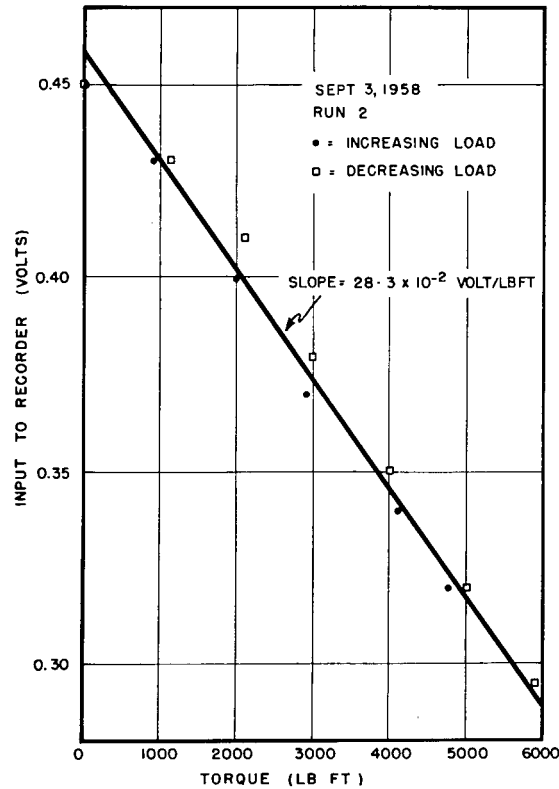


Fig. 12 - Calibration curve,
torque instrumentation

strain specimen. This was designed to survive loads caused by winds in excess of 80 knots, far faster than any wind speeds observed during these experiments.

Linearity - Hysteresis (probably caused by the friction in the elevation trunnion bearings) is the major nonlinearity. From Fig. 12, the width of the hysteresis loop is seen to be about 300 lb ft. The strain specimen would reach its proportional limit with winds greater than about 60 knots.

Frequency Response - The strain instrumentation should have a flat frequency response from zero to very high frequencies. The torque measurements, however, are affected by the transfer response of the antenna between the area of application of wind torque and the elevation crank arm. The lowest natural frequency of the antenna response to excitation about the elevation axis occurs at approximately 2.0 cps. Therefore, the transmission of torque to the elevation crank arm, and hence the torque measurements, are essentially flat out to about 1/2 cps, or 3.1 radians per second. (If necessary, a frequency calibration could have been made in order to extend the useful data out to 10 radians per second. This proved to be unnecessary, because practically no data were obtained beyond 3 radians per second.)

Drift - Standard techniques were used to minimize thermal drift of the strain-gage bridge. All four strain gages were taken from the same lot. Two gages made of the same material as the specimen and serving as passive arms of the bridge were mounted on a strip located as close as possible to the strain specimen. The gages were shaded from the direct rays of the sun by an aluminum cover.

Upon initial installation of the strain-measuring equipment, the output of the preloaded bridge exhibited a severe drift, especially when the sun was shining. When the preload was removed, however, the bridge returned to balance. This condition indicated that the drift was a measure of a changing strain in the specimen, explained qualitatively as follows. Figure 13a is an outline sketch of the H-beam mounted on the elevation crank arm. Figure 13b indicates schematically the relative positions of the neutral axis of the H-beam and of the crank arm. The heat of the sun would cause the temperature of the top of the H-beam to rise more rapidly than the temperature of its bottom. This would cause a downward deflection of the end of the H-beam, as indicated by a dashed line in Fig. 13b. A similar deflection can be expected to occur in the crank arm. The difference in the geometry and thermal characteristics of the two members will, in general, cause different rates of deflection. Thus, an initial end separation d_0 , Fig. 13b, becomes at some later time the separation d_1 . This relative deflection will, of course, induce a change of strain in the specimen of magnitude

$$\epsilon_2 = \frac{d_0 - d_1}{L_2}$$

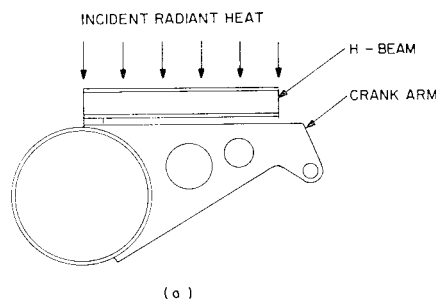
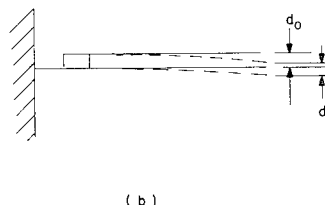


Fig. 13 - Thermal strain drift problem



It was not practical to provide effective thermal insulation for the entire elevation crank arm and H-beam assembly. This thermal drift, however, was greatly mitigated by the construction of an insulating box for the H-beam which served to match approximately its deflection rate with that of the crank arm. Figure 14 shows this box enclosing the equipment mounted on the crank arm. The exterior of this insulating box is also partially visible in Fig. 4. Thermal drift remained a problem throughout the tests whenever runs were made during periods of strong sunlight.

FIELD PROCEDURE

The field procedure was as follows:

1. Warm up equipment.
2. Calibrate with weight on H-beam.

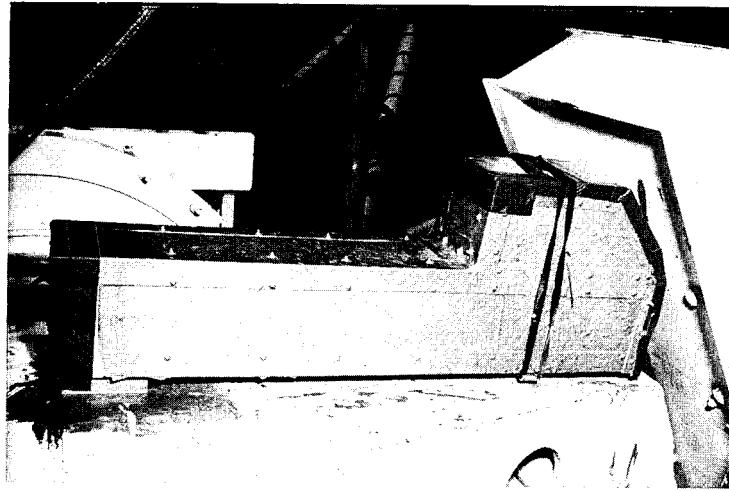


Fig. 14 - Strain-measuring equipment setup on antenna

3. Position antenna in azimuth and elevation to obtain desired position with respect to wind.
4. Preload strain specimen.
5. Record wind torque (bridge output), velocity, and direction for duration of run.

It was desired to obtain recordings of wind torque versus time with the antenna elevation angle set at zero, 45, and 90 degrees (zenith). With the antenna elevation angle at zero and 45 degrees respectively, runs were planned with the relative bearing of the wind approximately at zero, ± 45 , ± 90 , ± 135 , and 180 degrees. With the antenna pointing at the zenith, the symmetry renders runs at zero and 180 degrees equivalent, also 45 and 135 degrees. Fewer runs were therefore required for coverage at this elevation angle. It was desired to obtain at least two or three runs at each of these thirteen values of relative wind bearing. It was further desired to obtain a comparatively large number of runs at each of two or three relative bearings, so as to reveal functional relationships, if any, with observed wind characteristics. It was obviously desired to obtain these runs with as great a variety of wind conditions as possible, with emphasis on the higher wind velocities.

For each run, the specimen preload must be such as to satisfy the following requirements:

1. The strain-gage specimen must be always in tension during the run.
2. The tensile stress in the specimen must remain below its elastic limit and, if possible, below its proportional limit.
3. The modulation of the carrier must not exceed 100 percent in a downward direction for any appreciable part of the run.
4. The percentage modulation should be as high as possible, consistent with the other requirements.
5. The input voltage level at the recorder must remain within specified limits.

If the first requirement listed above is met, the third requirement will automatically be met. The second requirement was never a factor in the winds actually experienced, although with winds above 50 knots it would have become a limitation on the preload. The fifth requirement, recording level, could also be controlled by the amplitude of the bridge excitation from the signal generator (Fig. 7). The preload criteria therefore reduced to providing a preload great enough so that there seemed to be little likelihood of the amplifier output going to zero, yet small enough that the fluctuations in the wind would cause a significant modulation of the bridge output. The preload was set and locked using the preload control box, and the setting was monitored by means of the ac voltmeter, which indicated the output of the Ampex amplifier. A bridge excitation of 2 volts at 19.5 cps was used for most runs. This voltage was reduced for a few runs made during exceptionally strong winds in order to avoid exceeding the allowable input level for the recorder.

During the course of a run an observer would monitor the output of the Ampex amplifier in order to detect drift and to check the preload. During a number of runs, note was taken of the maximum output voltage observed.

A number of preliminary runs were recorded during September and October of 1958 using a tape speed of 3.54 inches per minute (ipm). Two runs, Nos. 60 and 61, were recorded during this period at a tape speed of 1.18 ipm. All of the later runs, mostly made during February, March, and April 1959, were recorded at this slower speed.

Table 1 lists the successful runs at 1.18 ipm in numerical order and displays the basic experimental conditions for each run: antenna elevation and azimuth angles, average wind speed and direction, and peak wind speed. Antenna azimuths relative to the wind are also listed in this table.

ANALYSIS

Spectrum Analysis of Recordings

The instrumentation for analysis of the tape recordings is shown in the block diagram, Fig. 15. A length of magnetic tape bearing the record of a run is spliced into a loop which is continuously played back by an Ampex recorder (model 302). The output of the playback amplifier is fed to a full-wave detector. The detector output is fed through a control panel to a General Radio wave analyzer, type 736-A. The analyzer tuning is scanned over the frequency range 0 to 500 cps by a motor drive. The output from the analyzer is recorded on paper tape by a Sanborn recorder (model 127). For some runs, the output of the detector was also fed through a blocking capacitor to a noise power meter.

In such a system, the frequencies of the recorded data are multiplied by the ratio of playback speed to recording speed. Playback speeds of 30 and 15 inches per second (ips) were available. Although the analyzer was arranged to scan the frequency interval 0-500 cps, it was actually effective only over the band from approximately 10 to 500 cps. Recording at 3.54 ipm and using the 30-ips playback speed, a real frequency range is obtained from 0.12 to 6.2 radians per second. Using the 15-ips playback speed with the same recording speed, the real frequency range becomes 0.24 to 12.4 radians per second. Thus, the equipment was capable of handling the frequency range originally postulated (0.1 to 10.0 radians per second).

As mentioned above, under "Field Procedure," a number of preliminary runs were recorded using the tape speed of 3.54 ipm. Analysis of these runs showed that all of the data (as played back at 30 ips) were concentrated in the frequency band below 150 cps. The recording speed was therefore reduced to 1.18 ipm for all subsequent runs in order to increase the frequency multiplication and thus make more effective use of the spectrum analyzer. The effective frequency range then became 0.04 to 2.1 radians per second at

Table 1
Summary of Wind Conditions

Run No.	Elevation Angle (Degrees)	Relative Bearing* (Degrees)	Average Wind Speed (Knots)	Peak Wind Speed (Knots)	Average Wind Direction (Degrees)	Antenna Azimuth (Degrees)
60	90	008	2.4	6.0	148	140
61	90	006	2.3	6.0	146	140
84	90	040	Not Rec.	10	180	140
85	90	168	6.5	17	332	140
86	90	173	7.7	17	327	140
87	90	176	6.8	17	324	140
88	90	171	9.8	26	329	140
93	0	166	11.3	35	327	133
95	0	174	11.7	30	319	133
96	0	100	10.8	26	321	221
97	0	049	9.7	23	316	267
98	45	177	9.6	20	310	133
99	45	164	8.5	22	329	133
100	0	054	7.9	15	319	265
101	45	043	7.5	14	308	265
102	0	164	6.7	13	284	120
106	0	012	7.0	15	198	210
107	0	014	6.7	18	196	210
112	45	180	11.9	24	315	135
113	45	179	12.9	30	314	135
114	0	178	10.0	24	317	135
115	0	179	8.7	24	316	135
116	45	175	8.8	20	320	135
117	45	179	5.8	16	314	135
118	0	138	5.5	20	318	180
119	0	137	6.9	22	317	180
120	45	084	10.2	20	336	060
121	45	086	8.0	20	334	060
122	0	085	8.0	20	335	060
124	0	124	9.0	19	334	210
127	0	-25 and +35	2.4	4.5	330 and 030	355

* Bearing of antenna relative to wind.

Table 1 (Continued)
Summary of Wind Conditions

Run No.	Elevation Angle (Degrees)	Relative Bearing* (Degrees)	Average Wind Speed (Knots)	Peak Wind Speed (Knots)	Average Wind Direction (Degrees)	Antenna Azimuth (Degrees)
129	0	030	3.9	13.5	190	160
130	45	000	3.3	12.8	190	190
131	45	009	4.6	16.5	346	355
132	0	174	4.5	15	206	020
133	0	008	4.1	14.3	208	200
134	45	146	5.9	15	211	065
135	45	141	5.8	19	206	065
136	45	045	5.8	18	215	170
137	45	048	5.1	16	224	272
138	45	008	5.2	11.3	352	000
139	45	023	3.4	11.3	337	000
140	45	025	1.5	6.0	025	000
142	0	012	1.4	8.2	042	030
144	0	040	3.1	9.0	350	030
146	0	033	4.8	16	321	354
148	0	030	5.6	16.5	324	354
149	0	173	6.1	18	322	135
150	0	177	5.2	17	318	135
151	90	079	0.7	4.5	219	140
152	90	071	0.0	1.0	211	140
153	0	157	0.0	1.1	157	000
154	0	152	0.7	5.3	152	000
155	0	119	2.4	9.0	119	000
156	0	155	5.0	14	345	190
157	0	177	4.9	15	343	160
158	0	178	1.5	6.0	018	200
160	0	164	1.5	4.5	004	200
161	0	015	0.8	3.7	014	359
162	0	001	1.9	6.0	000	359

* Bearing of antenna relative to wind.

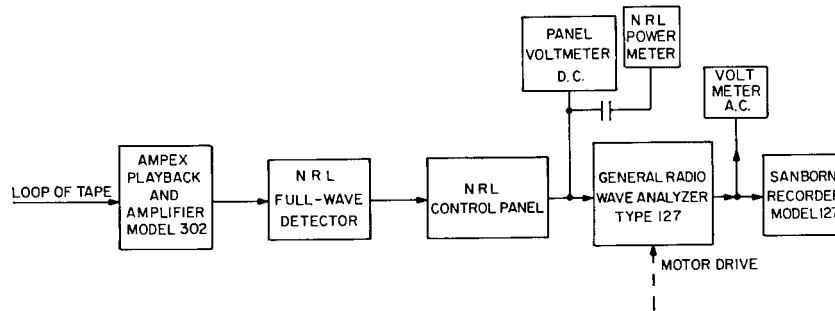


Fig. 15 - Block diagram of instrumentation for spectrum analysis of recordings

30-ips playback speed. In order to provide a sufficient length of tape to operate as a loop with this equipment, runs of about 40 minutes duration were made. After cutting and splicing, each tape contains data for a run of about 33 minutes. Since the period corresponding to the lowest frequency is 157 seconds, this time of 33 minutes is sufficient for more than 12 complete cycles, an adequate figure for recording and analysis.

This analysis is based upon the inexact, but practical, assumption that the statistics of the wind do not change during a run.

Other Analysis

Wind - The average velocity of the wind for each run was determined by reading the tape from the wind recorder at 30-second intervals and taking the arithmetical average of these readings. During several runs, when the speed recorder was inoperative, the wind indicator was read directly and noted at 30-second intervals.

The wind-direction record from the recorder was averaged by eye over short intervals appropriate to the character of the particular record. The arithmetical average of these interval averages was then obtained for the run.

An example of the wind recorded at this site is displayed in Fig. 1. The upper record shows the wind direction for three minutes out of Run No. 132. The lower record shows the wind speed during the same period.

Torque Data - The output of the spectrum analyzer for each run is a curve of voltage amplitude versus frequency for the output of the strain-gage bridge. The analyzer outputs for several typical runs are shown in Figs. 16 and 17. A plot of the mean-squared torque density spectrum is desired for each run. To obtain this curve, the analyzer output curve is squared, point by point, and replotted, after correcting for analyzer bandwidth, calibration factors, gain settings, etc.

The area under the torque spectral density curve represents the mean-squared value, for the duration of the run, of the portion of the wind-torque spectrum lying within the passband of the instrumentation. Since this instrumentation is more than adequate at the high-frequency end of the spectrum, it can be said that the area under the torque spectral density curve equals the rms value of all components of the wind-torque spectrum lying above 0.04 radians per second. The areas were obtained by numerical integration without actually plotting the curves on linear paper.

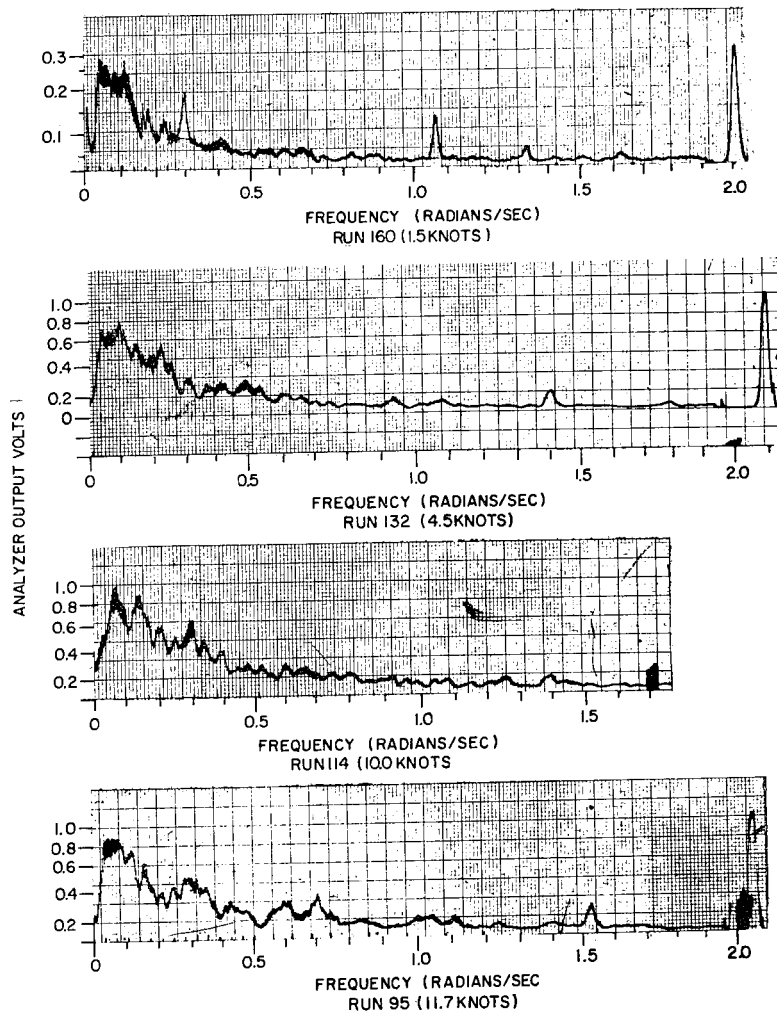


Fig. 16 - Typical recordings of spectrum-analyzer output, elevation 0°

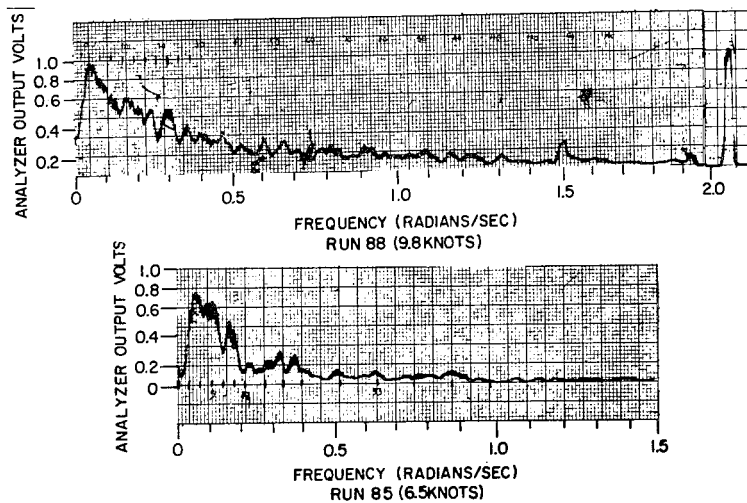


Fig. 17 - Typical recordings of spectrum-analyzer output, elevation 90°

A mathematical expression for the torque-density spectrum is desired in order to use this type of data in the analysis of a servo system. For each run, the equation for this quantity was obtained by curve fitting on a log-log plot of torque spectral density versus frequency. This process was based on the following two hypotheses: (a) since the function is obtained by a squaring process, the slopes of the asymptotes of the plots will be even numbers, and (b) the low-frequency slope must be zero, because the torque at zero frequency cannot be infinite.

The equation for torque spectral density must therefore be of the form

$$\Phi_{TT} = K \left(\frac{\omega_0^2}{\omega_0^2 + \omega^2} \right) \left(\frac{\omega_1^2}{\omega_1^2 + \omega^2} \right) \left(\frac{\omega_2^2}{\omega_2^2 + \omega^2} \right) \dots \quad (8)$$

Inspection of the log-log graphs of the 60 satisfactory runs reveals that the function whose asymptotes are indicated in Fig. 18a seems to provide a good fit to the data for most runs. The torque spectral density would therefore be expressed in the form

$$\Phi_{TT} = K \left(\frac{\omega_0^2}{\omega_0^2 + \omega^2} \right). \quad (9)$$

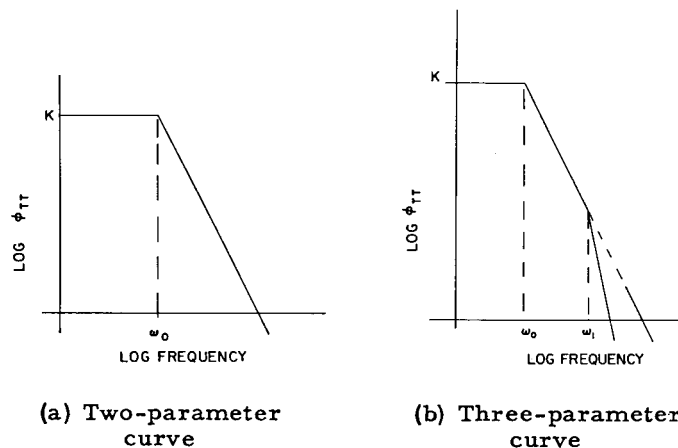


Fig. 18 - Asymptotes of spectral-density curve

A function of this form is used by Newton and others.* The log-log graphs of four of the runs shown on Figs. 16 and 17 are plotted on Fig. 19. On each of these graphs, a curve is drawn satisfying Eq. (9). The asymptotes and the values of K and ω_0 are indicated.

It can be seen from Fig. 19 run 95, that there is evidence of a high-frequency corner, ω_1 , occurring at about 1.5 radians per second, with a minus-4 slope at higher frequencies. This would suggest a function with asymptotes as indicated on Fig. 18b. A large number of the other runs (not reproduced here) seem to indicate a similar high-frequency corner. These data, however, do not clearly define the corner, because it occurs too close to the

*Newton, Gould, and Kaiser, op. cit. p. 259.

D. K. Barton, "Final Report, Instrumentation Radar AN/FPS-16 (XN2)," Radio Corporation of America, Moorestown, N. J., Feb. 27, 1959.

Moll, Kirschbaum, Wetherbee, and Weimer, "Results of Computations on Wind-Velocity Data," Battelle Memorial Institute, Columbus, Ohio, April 15, 1959.

upper limit of the frequency range obtained at the 30 ips playback speed. By playing the tapes back at a slower speed, it should be possible to obtain a better picture of the high-frequency end of the spectrum and to identify the frequency of this second corner. Three tapes were therefore played back at 15 ips as well as at 30 ips. Values for this second corner frequency, ω_1 , ranging from 1.6 to 2.4 radians per second were obtained for runs 88, 93, and 116. Log-log plots of Φ_{TT} vs ω for these runs are shown in Fig. 20.

It is concluded, then, that torque spectral density can be more precisely expressed in the form

$$\Phi_{TT} = K \left(\frac{\omega_0^2}{\omega_0^2 + \omega^2} \right) \left(\frac{\omega_1^2}{\omega_1^2 + \omega^2} \right). \quad (10)$$

RESULTS

Continuous recordings of the wind-induced elevation torque were obtained for 60 runs of about 40 minutes duration. After the magnetic tapes had been trimmed and spliced into loops, each run represented 33 minutes; thus the total time represented by the data reported here is 32.5 hours. The peak reading of the wind speed during these runs was 35 knots. The maximum average speed over any complete run was 12.9 knots. The speed of the fastest mile of air was about 20 statute miles per hour. As noted above, the experimental conditions for these runs are summarized in Table 1.

The values obtained for the principal characteristics of the torque-density curves are listed in Table 2, wherein each row sets forth the results of a single run. In this table, the runs are separated into 14 groups according to antenna elevation angle and bearing angle relative to the wind. The grouping follows the plan outlined under "Field Procedure." The bearing demarcation between groups with 45 or 0 degrees elevation angle is shown on Fig. 21. In the case of 90-degree elevation, groups I and V are identical, as are groups II and IV. The observed elevation and relative bearing angles are given for each run in the columns numbered 1 and 2 of the table.

Within each group, runs are listed in order of the observed average wind speed, column 3. The observed peak wind speeds are listed in column 4. The quantity K and the corner frequency ω_0 defined by Fig. 19 are listed in columns 5 and 6, respectively. The product $K\omega_0$, taking proper cognizance of the units involved, is tabulated in column 7. The root-mean-square value of the torque within the band from 0.04 to 2 rad/sec is given in column 8. The observed wind direction, believed to have a major effect upon the wind-speed measurements, is given in column 9.

Relations Between Spectral-Density Characteristics and Wind Velocity

Results taken from Table 2 have been plotted in Figs. 22 through 27 in order to demonstrate the functional relationship, if any, between the quantity $K\omega_0$ and the average wind speed observed. Since instantaneous wind torque is proportional to the square of the velocity, and since the quantity $K\omega_0$ has the dimensions of torque squared per cycle per second, it would be expected that the quantity $K\omega_0$ would have a magnitude proportional to the fourth power of wind velocity. Figures 22 through 27 show log-log plots of $K\omega_0$ versus average wind speed, with a straight line drawn through each set of data to represent this fourth-power relationship. It can be seen that the five groups of data plotted on Figs. 23 through 25 and Fig. 27 conform substantially to such a straight line, although the data on Figs. 22 and 26 show a rather wide spread.

NAVAL RESEARCH LABORATORY

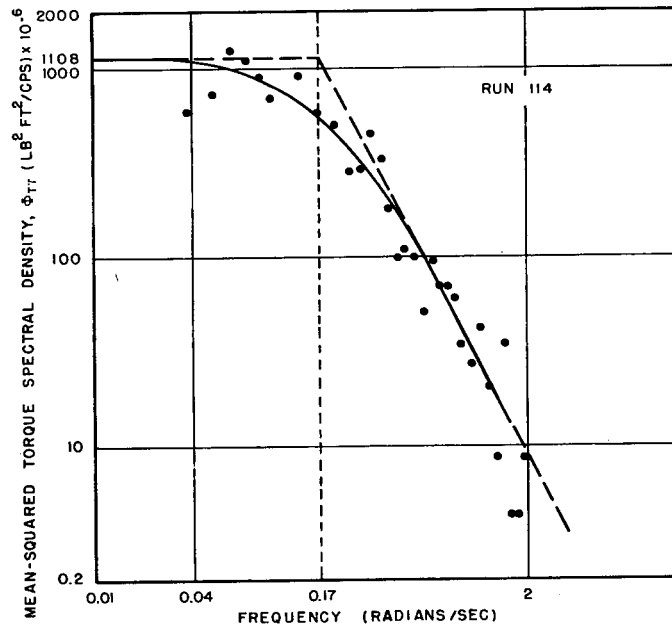
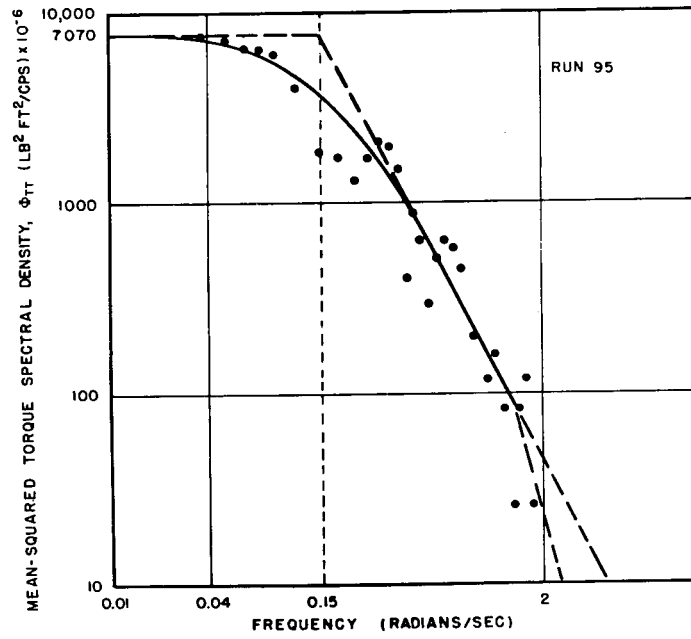


Fig. 19 - Log-log plots of torque spectral density vs frequency

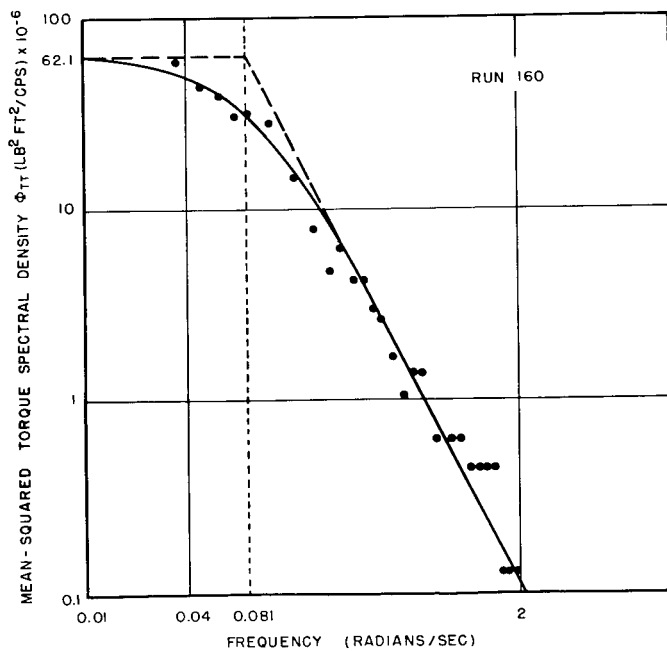
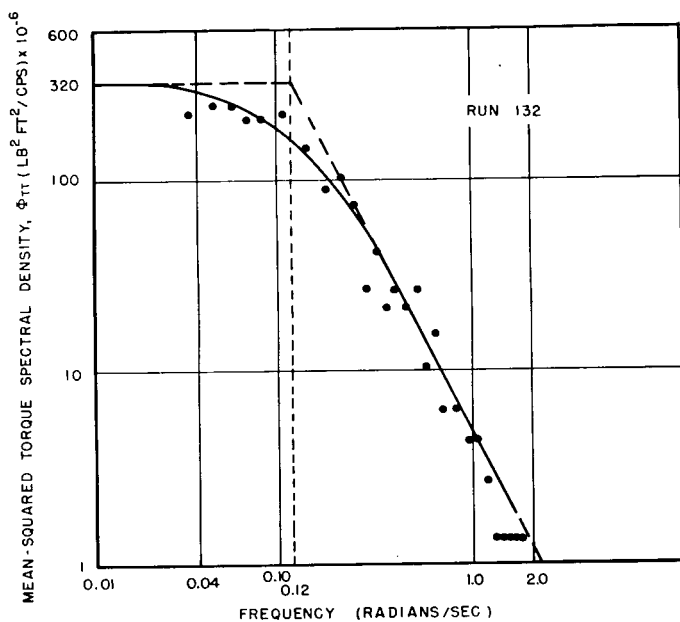


Fig. 19 (Continued) - Log-log plots of torque spectral density vs frequency

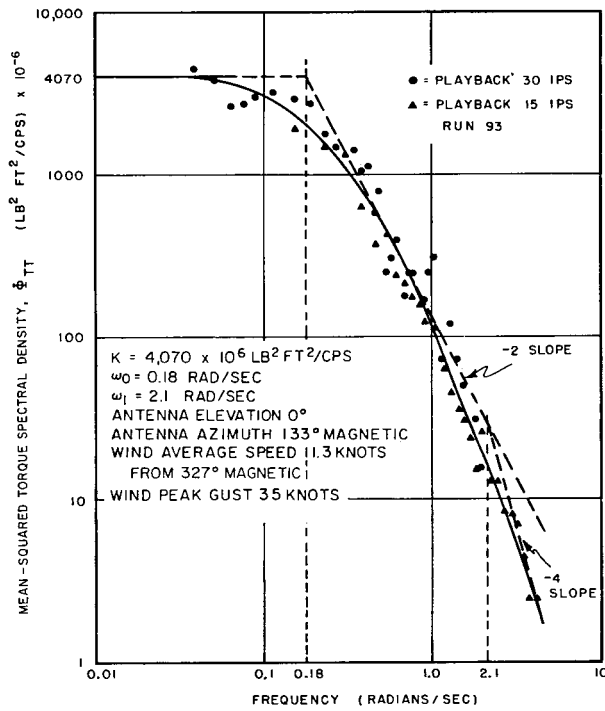
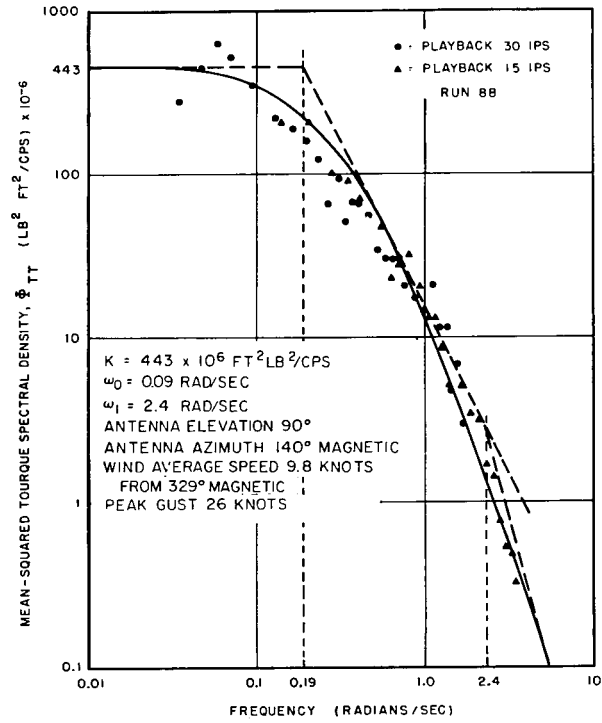
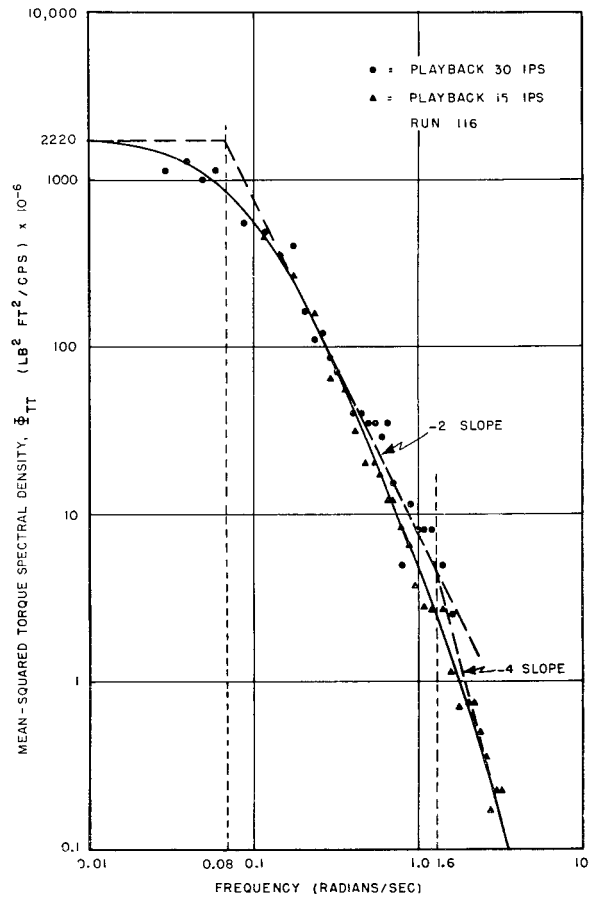


Fig. 20 - Log-log plots of torque spectral density, runs 88, 93, and 116



$K = 1,890 \times 10^{10}$
 $\omega_0 = 0.082 \text{ RAD/SEC}$
 $\omega_1 \pm 1.6 \text{ RAD/SEC}$
 ANTENNA ELEVATION 45°
 ANTENNA AZIMUTH 135°
 WIND AVERAGE SPEED 8.8 KNOTS FROM 320° MAGNETIC
 PEAK GUST 20 KNOTS

Fig. 20 (Continued) - Log-log plots of torque spectral density, runs 88, 93, and 116

Table 2
Summary of Mean-Squared Torque Density Spectrum Characteristics
Data Grouped by Antenna Orientation

0	1	2	3	4	5	6	7	8	9	10
Relative Azimuth Group	Elevation Angle (Degrees)	Relative Bearing (Degrees)*	Average Wind Speed (Knots)	Peak Wind Speed (Knots)	$K \times 10^{-6}$ (lb ² ft ² /cps)	$\omega_0 \times 10^2$ (rad/sec)	$K\omega_0 \times 10^{-6}$ (lb ² ft ²)	Torque rms (lb ft)	Average Wind Direction (Degrees)	Run No.
I	0	015	0.8	3.7	37.2	9.6	0.569	418	014	161
	0	012	1.4	8.2	32.8	10.3	0.539	809	042	142
	0	001	1.9	6.0	15.5	13	0.321	377	000	162
	0	000	2.4	4.5	15.5	11.5	0.284	629	000	127
	0	030	3.9	13.5	247	10.9	4.29	2110	190	129
	0	008	4.1	14	62	29	2.87	2060	208	133
	0	030	5.6	16.5	78.2	21.8	2.72	1934	324	148
	0	014	6.7	18	80.4	24	3.07	2230	196	107
	0	012	7.0	15	144	18	4.13	2335	198	106
II	0	040	3.1	9.0	28.5	7.7	0.350	650	350	144
	0	033	4.8	16	114.1	16	2.91	1948	321	146
	0	054	7.9	15	125	24	4.78	2490	319	100
	0	049	9.7	23	1300	13.3	27.6	5180	316	97
III	0	085	8.0	20	80.6	17	2.18	1610	335	122
	0	100	10.8	26	1212	16	30.9	5990	321	96
IV	0	119	2.4	9.0	80.6	3.9	0.501	630	119	155
	0	138	5.5	20	105	21	3.52	2055	318	118
	0	137	6.9	22	192	18	5.51	2690	317	119
	0	124	9.0	19	118	21	3.95	2290	334	124
V	0	157	0.0	1.1	46.7	7.3	0.543	778	157	153
	0	152	0.7	5.3	45.2	9.3	0.670	901	152	154
	0	164	1.5	4.5	62.1	8.1	0.803	534	004	160
	0	178	1.5	6.0	164	6.3	1.64	1316	018	158
	0	174	4.5	15	320	12	6.12	2760	206	132
	0	177	4.9	15	305	12	5.83	2820	343	157
	0	155	5.0	14	159	16	4.05	2450	345	156
	0	177	5.2	17	266	8.5	3.61	2130	318	150
	0	173	6.1	18	1142	6.3	11.5	3380	322	149
	0	164	6.7	13	381	7.9	4.79	2220	284	102
	0	179	8.7	24	1441	18	41.5	6470	316	115
	0	178	10.0	24	1108	17	30.0	5980	317	114
	0	166	11.3	35	4070	18	117.8	13320	327	93
	0	174	11.7	30	7070	15	169	13570	319	95

*Bearing of antenna relative to wind.

Table 2 (Continued)
 Summary of Mean-Squared Torque Density Spectrum Characteristics
 Data Grouped by Antenna Orientation

0	1	2	3	4	5	6	7	8	9	10
Relative Azimuth Group	Elevation Angle (Degrees)	Relative Bearing (Degrees)*	Average Wind Speed (Knots)	Peak Wind Speed (Knots)	$K \times 10^{-6}$ (lb ² ft ² /cps)	$\omega_0 \times 10^2$ (rad/sec)	$K\omega_0 \times 10^{-6}$ (lb ² ft ²)	Torque rms (lb ft)	Average Wind Direction (Degrees)	Run No.
I	45	025	1.5	6.0	70.8	9.7	1.09	989	025	140
	45	000	3.3	12.8	168.2	11.5	3.08	1219	190	130
	45	023	3.4	11.3	86.3	7.9	1.09	1088	337	139
	45	009	4.6	16.5	347.5	5.3	2.93	1766	346	131
	45	008	5.2	11.3	203	9.7	3.14	1850	352	138
II	45	048	5.1	16	143	10.9	2.48	1665	224	137
	45	045	5.8	18	216	8.5	2.93	1720	215	136
	45	043	7.5	14	263	6.8	2.85	1584	308	101
III	45	086	8.0	20	1021	18	2.93	1803	334	121
	45	084	10.2	20	1388	17	37.6	1936	336	120
IV	45	141	5.8	19	256	9.7	3.95	2145	206	135
	45	146	5.9	15	202.5	12	3.88	2270	211	134
V	45	179	5.8	16	1060	9.9	16.7	3930	314	117
	45	164	8.5	22	1193	18	34.2	6670	329	99
	45	175	8.8	20	2220	8.2	29.0	5670	320	116
	45	177	9.6	20	3710	9.1	53.8	8080	310	98
	45	180	11.9	24	1278	9.7	19.7	4700	315	112
	45	179	12.9	30	860	13	17.8	4875	314	113
I	90	006	2.3	6.0	17.28	9.1	0.250	360	146	61
	90	008	2.4	6.0	7.79	12.1	0.152	289	148	60
V	90	168	6.5	17	477	7.3	5.55	2290	332	85
	90	176	6.8	17	588	7.9	7.40	3070	324	87
	90	173	7.7	17	354	9.1	5.13	2370	327	86
	90	171	9.8	26	443	19.4	13.7	3705	329	88
II	90	040	Not Rec.	10	49.4	8.9	0.700	912	180	84
III	90	071	0.0	1.0	359	2.9	1.66	1088	211	152
	90	079	0.7	4.0	67.9	6.0	0.649	877	219	151

* Bearing of antenna relative to wind.

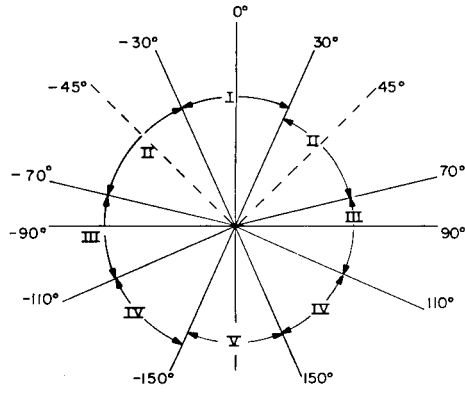


Fig. 21 - Relative bearing grouping diagram

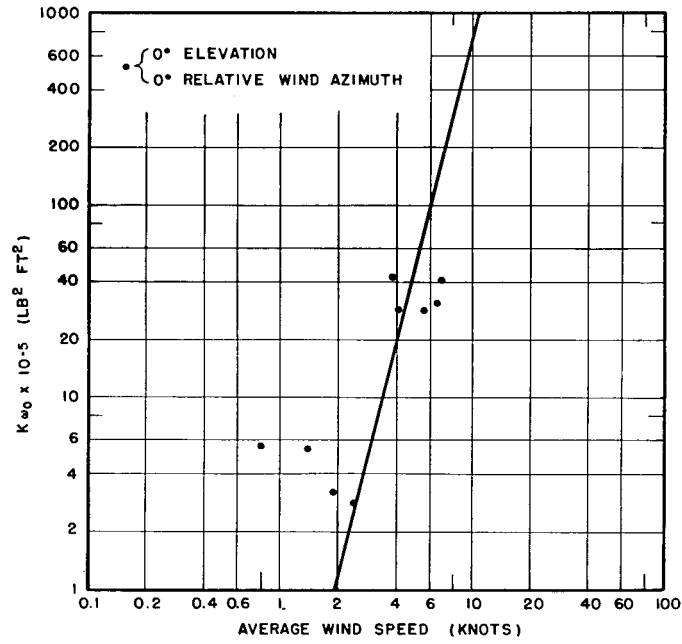


Fig. 22 - Log-log plot of amplitude-bandwidth product vs average wind speed, 0° elevation, Group I

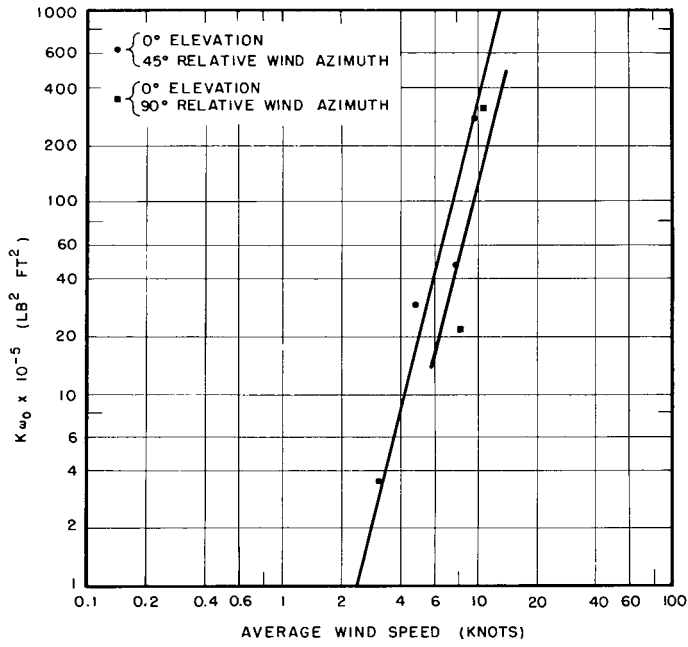


Fig. 23 - Log-log plots of amplitude-bandwidth product vs average wind speed, 0° elevation, Groups II and III

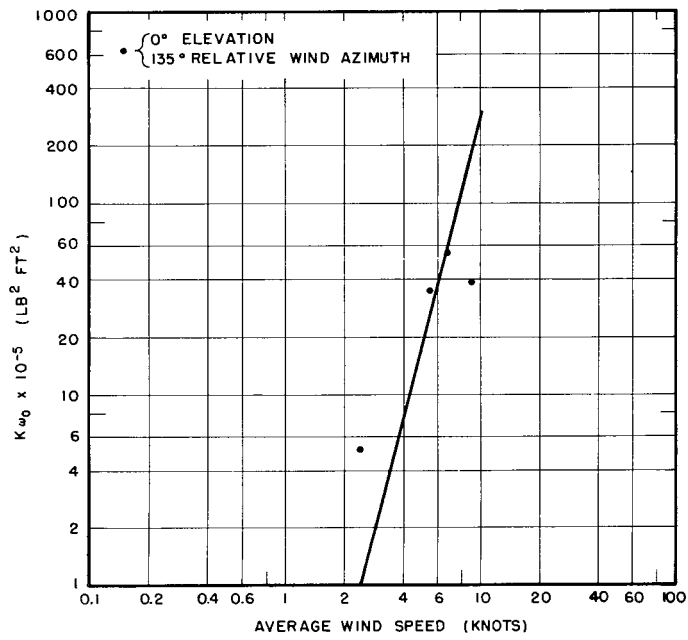


Fig. 24 - Log-log plot of amplitude-bandwidth product vs average wind speed, 0° elevation, Group IV

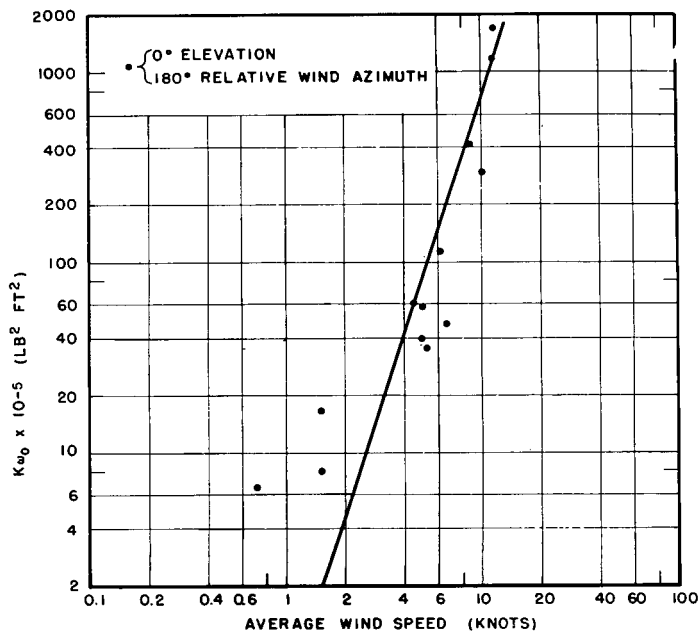


Fig. 25 - Log-log plot of amplitude-bandwidth product vs average wind speed, 0° elevation, Group V

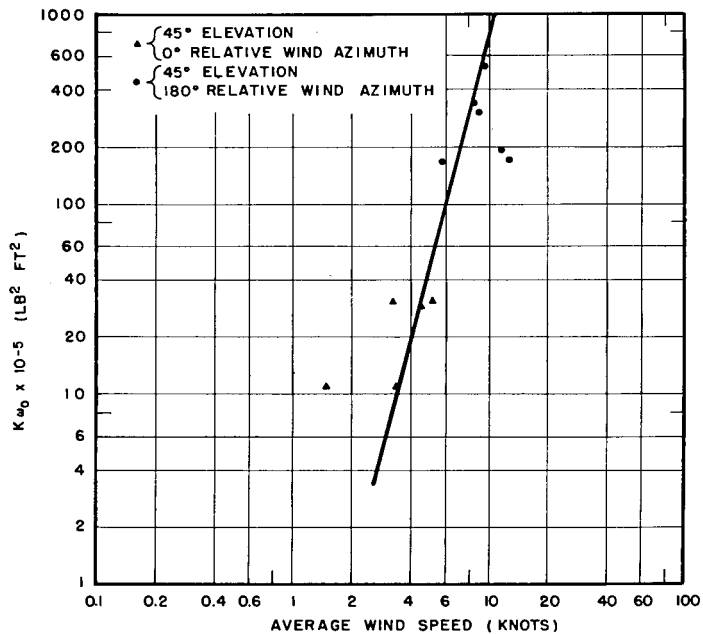


Fig. 26 - Log-log plots of amplitude-bandwidth product vs average wind speed, 45° elevation, Groups I and V

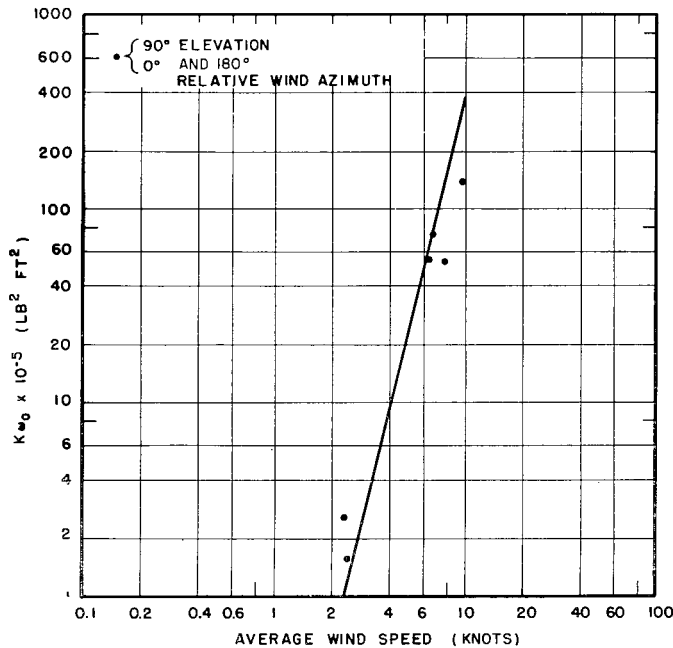


Fig. 27 - Log-log plots of amplitude-bandwidth product vs average wind speed, 90° elevation, Groups I and V

The values obtained for the first corner frequency, ω_0 , range from 0.029 to 0.29 radian per second, with an average value of 0.12 and a median value of 0.11. No clear functional relationship between ω_0 and wind speed was observed. If this frequency ω_0 is indeed independent of wind speed the factor K must evidently be also proportional to the fourth power of the velocity. Values of ω_0 are plotted vs wind speed in Appendix B.

Moment Coefficients

A reasonably accurate knowledge of the moments and torques exerted by the wind is essential to the design of the structure and the power drives of a large antenna. Although static torque figures were not originally listed as an objective of this study, it was found possible to associate the velocity records of 13 particular wind gusts with peak torque values which had been observed during certain runs. These wind velocities, the resulting peak torques measured, and other related data are presented in Table 3.

The aerodynamic torque acting on a porous body of known geometry, such as an antenna with reflector of expanded metal, is sometimes calculated by the following straightforward procedure. A wind-velocity profile across the reflector surface is hypothesized (Fig. 28). Using drag coefficients based on wind-tunnel data, the force exerted by the wind on any element of the surface can be calculated. The torque exerted about any desired axis can then be found by multiplying the force on each element by its effective moment arm and integrating over the entire surface of the reflector. The worst difficulty in the practical use of this procedure lies in the assumption of a realistic wind profile. Because of the square-law relation between wind velocity and aerodynamic force, moderate changes in the assumed profile will yield substantial differences in the calculated torque value.

Table 3
Moment Observations and Moment Coefficient

Run No.	Elevation Angle (Degrees)	Relative Bearing* (Degrees)	Wind Speed† (Knots)	Wind* Direction (Degrees)	Maximum Moment (lb ft)	C_m
93	0	166	35	327	172,000	0.24
93	0	166	24	327	72,300	0.22
132	0	174	10	206	17,500	0.30
160	0	164	4	004	2,040	0.22
133	0	008	14.3	208	19,430	0.16
129	0	030	13.5	190	17,650	0.17
148	0	030	12	324	11,230	0.170
127	0	035	4.5	030	2,480	0.21
130	45	000	12.8	190	12,380	0.13
136	45	045	20	215	17,500	0.076
137	45	048	14	224	7,070	0.062
134	45	146	15	211	19,430	0.15
134	45	146	12	211	14,120	0.17
88	90	171	26	329	33,300	0.085

* Average value for run.

† Velocity at instant that torque was noted; usually a peak.

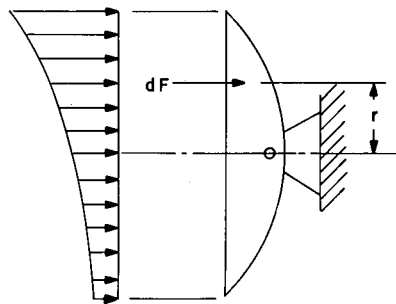


Fig. 28 - Hypothetical vertical profile of wind speed acting on antenna

In wind-tunnel work with aerodynamic shapes, use is made of the equation

$$M = C_M qSL \quad (11)$$

where

- M = torque (lb ft)
- S = characteristic area of body (ft²)
- C_M = moment coefficient
- q = 1/2 ρV² (lb/ft²)
- L = characteristic length of body
- ρ = 0.00238 lb sec²ft⁻⁴ (density of air)
- v = velocity (ft/sec)

The moment coefficient derived in most wind-tunnel work is determined by the geometry of the body and its aspect angle relative to the uniform air velocity. To a lesser extent, C_M is a function of the Reynolds number of the air flow, and hence of the velocity.

Values of C_M derived from the values of v_T and M_{m ax} listed in Table 3 by using Eq. (11) are listed in the last column of the table. It will be noted that within each of the first two groups of data, which are grouped by similar aspect angles, the values of C_M are quite consistent, except for the high value obtained from run 132. This value can possibly be accounted for by the position of the aerovane, which was behind the antenna for the combination of wind direction and antenna azimuth prevalent during run 132. (If the true value of wind speed, v_T were 12 knots, rather than the 10-knot value recorded, the calculated value of C_M for this run would have been 0.210.)

The values of C_M obtained here, in contrast to wind-tunnel-derived values, are determined to a considerable degree by the prevailing wind structure at the site and are therefore strictly applicable only to this particular antenna at this particular site. It seems reasonable to believe, however, that if wind-torque measurements were taken on similar antennas at several different sites, a body of design information would become available which could provide a basis for design which would be much more reliable than the use of an assumed wind profile.

Root-Mean-Square Torque Data

Data regarding the rms values of the variable component of the wind-induced torque would become essential if antenna designers were to consider fatigue in their design studies. The rms torque data listed for each run on Table 2 are plotted by groups in Figs. 29 through 32. These values, which could be used in servo analysis as an effective alternate to K, were obtained directly by numerical integration of the mean-square torque density spectrum over the effective real-time frequency interval of the analyzer and application of the appropriate scale factors. As an alternative, the rms torque could have been obtained by analytical integration of Eq. (9).

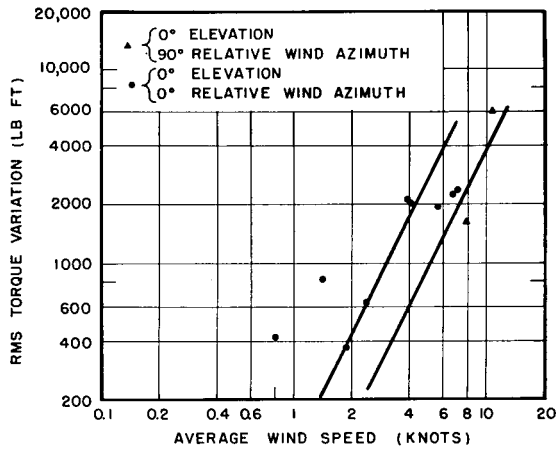


Fig. 29 - Log-log plots of rms torque variation vs average wind speed, 0° elevation, Group III, and Group I

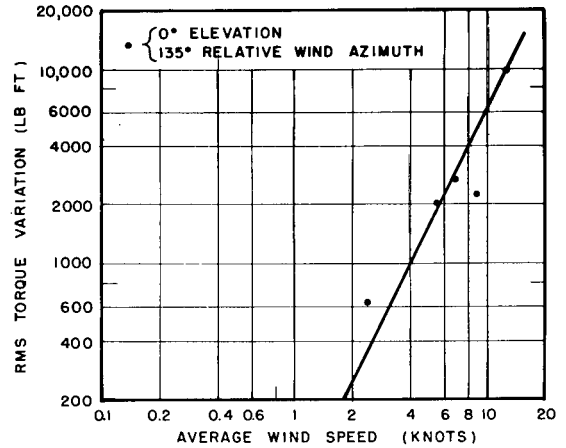


Fig. 30 - Log-log plot of rms torque variation vs average wind speed, 0° elevation, Group IV

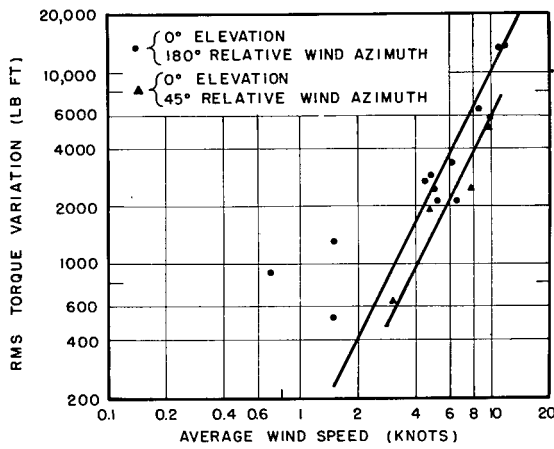


Fig. 31 - Log-log plots of rms torque variation vs average wind speed, 0° elevation, Groups II and V

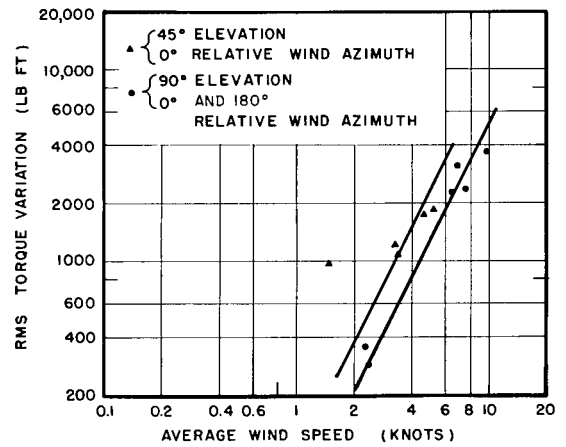


Fig. 32 - Log-log plots of rms torque variation vs average wind speed, 45° elevation, Group I, and 90° elevation, Groups I and V

Let T_{rms} = rms value of elevation torque.

Then

$$T_{rms} = \sqrt{\int_{\omega_1}^{\omega_2} \Phi_{TT} d\omega} = \sqrt{K \omega_0 \left(\tan^{-1} \frac{\omega_2}{\omega_0} - \tan^{-1} \frac{\omega_1}{\omega_0} \right)} \quad (12)$$

where

ω_1 = lower limit of effective operation of analyzer = 0.04 rad/sec

ω_2 = upper limit of effective operation of analyzer = 2.0 rad/sec.

The value of ω_0 varies from run to run, as noted above. Using the average of all values of this quantity listed in column 6 of Table 2 ($\omega_0 = 0.123$), Eq. (12) becomes

$$T_{rms} = \sqrt{1.20 K \omega_0}. \quad (13)$$

As would be expected, each group of data points plotted in Figs. 29 through 32 can be approximated (on log-log paper) by a straight line. Thus,

$$T_{rms} \simeq T_0 V^2 \quad (14)$$

where T_0 is the value of T_{rms} at 1 knot.

Values of T_0 can be obtained from the data for five different relative azimuth angles, with the antenna in each case at zero elevation angle. The variation of this torque constant with relative wind azimuth is shown and compared with a cosine-squared curve on Fig. 33. It will be noticed that the ordinate of the point plotted at 90 degrees azimuth is substantially greater than zero. This would be expected, when it is remembered that the wind direction varied substantially during the course of the two runs (Nos. 96 and 122) which provided the data for this point. During run 96, for example, the relative direction of the wind fluctuated almost continually between 79 and 139 degrees, with a few gusts from angles as widely dispersed as 14 and 179 degrees relative. The character of run 122 was similar.

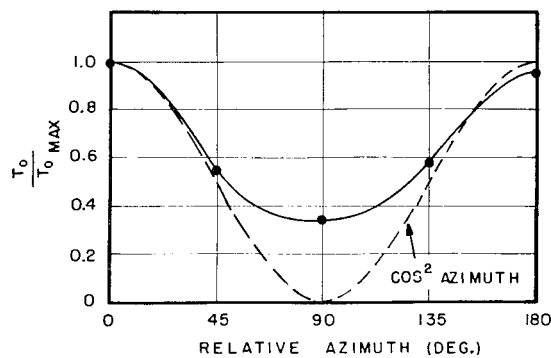


Fig. 33 - Variation of torque constant with relative wind azimuth, 0° elevation angle

Limitations of Results

The principal limitations of the data presented, in the stated frequency range of 0.04 to 2.0 rad/sec, are as follows:

1. Limited range of wind conditions represented
2. Thermal drift
3. Uncertainty of preload determination
4. Wind instrumentation
5. Processing noise.

The period of data collection included the latter part of February and the "windy months" of March and April. During this period, an effort was made to have a crew on hand to collect data whenever fresh or strong winds were predicted, regardless of time. Nevertheless, observed duration of strong winds was enough to permit only a few runs under those conditions. No gales were observed.

The distribution of wind peak- and average-velocity conditions for the 60 successful runs are indicated respectively in Figs. 34 and 35. It can be seen that peak velocities greater than 25 knots occurred during only five runs and that average velocities of 10 knots or greater occurred during seven runs.

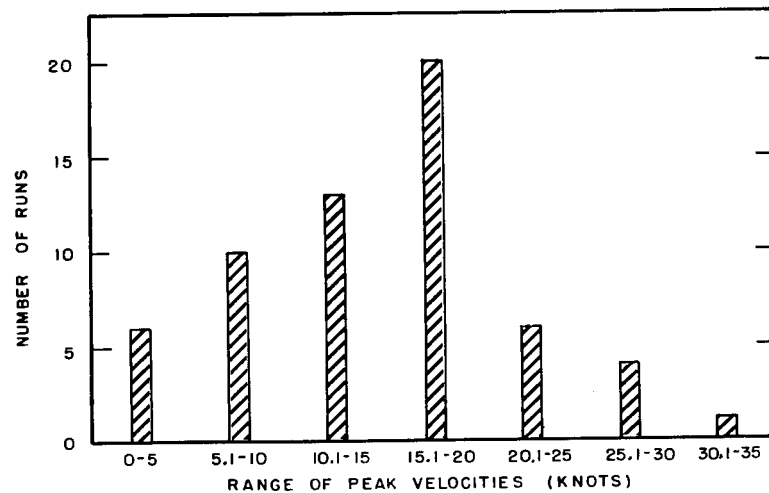
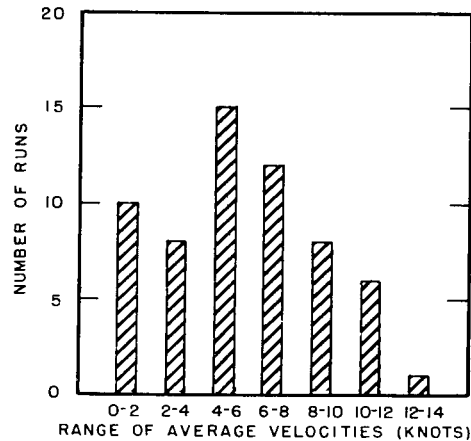


Fig. 34 - Frequency distribution of run peak velocity

If the drift caused by the relative thermal strain between the elevation torque-arm and the H-beam were to proceed at a uniform rate, the resulting ramp-type output from the strain-gage bridge would appear at the analyzer as a sawtooth with a real time period of about 32 minutes. The period corresponding to the lowest frequencies read from the analyzer is about 2.6 minutes. Thus the 13th and higher harmonics, representing about 6 percent of the energy of the signal from this ramp-type drift, would lie within the band of frequencies considered. During some of the runs characterized by light winds, it was possible to note the drift in some detail. In certain cases, such as run 134, the fundamental

Fig. 35 - Frequency distribution of run average velocity



drift period was a fraction of 32 minutes. In these cases, the action of drift would put a very appreciable signal within the pass band of the analyzer.

It may be noted that in Figs. 22, 25, and 26, the points representing data from runs with extremely low average wind speeds all stand far above the lines drawn to represent the consensus of the data. This can be in part attributed to thermal drift. The remainder of the discrepancy is probably caused by the lack of precision of the wind instrumentation as well as the limitations inherent in the attempt to represent the wind velocity over an area by measurements taken at a single point.

The instrumentation described permits the magnitude of the preload voltage to be observed only when the wind velocity drops to zero. This happened with sufficient frequency not to cause any particular delay in the taking of data, except on the one or two days with the strongest winds. Even on these occasions, it was found that the wind never failed to drop nearly to zero at some moment during the 40-minute run. This appeared to give sufficient knowledge of the preload to determine that the permissible limits of modulation were not exceeded.

It is evident that the single anemometer gives a strictly limited description of the wind occurring at the site. In particular, when the wind blew from southerly directions, the anemometer was partially blanketed by the antenna. (See the site plan, Fig. 5.) A majority of the runs, however, were made with winds from northerly and westerly directions (Table 1).

Application of Results

In the absence of more directly applicable data, there would be some reason to attempt extrapolation of some of these results to apply to other antennas. For example, the maximum torque figures might be used to check elevation-torque requirements at a given design wind velocity. The values of C_M from Table 3 could be used, with some caution, paying due regard to the differences in surface material and in structural arrangement. Probably the greatest risk in this extrapolation lies in the difference in wind-velocity profiles and distributions which may exist between different sites. It is felt that this site probably has rather extreme velocity differentials for a given reference velocity; therefore use of the values of C_M derived here will probably be conservative.

In using the torque-density spectrum data for predicting servo errors for other antennas, the factor K should be scaled by the ratio between the respective antenna diameters raised to some power ranging between 6 and 6-4/7, and by the fourth power of the average

wind velocity considered. (See Figs. 22-27.) The frequency parameter ω_0 could be chosen after referring to the plots in Appendix B. At present, there does not seem to be evidence of any effect of antenna size upon the value of ω_0 .

Moll, et al.,* have used wind-velocity data provided by Smith and Singer of Brookhaven National Laboratories to compute the rms value of wind-torque variation for the 600-ft paraboloid to be built at the Naval Radio Research Station, Sugar Grove, West Virginia. The wind data represented nine different runs, each of about 20 minutes duration. Using a value of $C_D = 0.55$, they calculated rms torques for the different runs ranging from 18×10^6 to 74×10^6 lb ft, based upon a 26-knot wind at a 50-ft elevation.

The data of Fig. 29 were used to calculate the corresponding rms variation in wind torque acting on a 600-ft-diameter reflector having the same drag coefficient as the antenna at Stump Neck, Maryland. If the diameter ratio between the two antennas is raised to the third power in this calculation, an rms torque value of 68×10^6 lb ft is obtained; for an exponent of $3-2/7$, the value becomes 130×10^6 lb ft. Considering the possible difference in drag coefficients, and the tremendous extrapolation factor involved ($10^{3.286} = 1930$), these answers seem to be in fair agreement. (This example is quoted merely because of the availability of published figures for comparison. It would not be recommended that extrapolations of the present data be used in the design of a 600-ft antenna without very careful interpretation.)

It will be recalled that the introduction to this report discusses a method of obtaining a torque-density spectrum by the simple process of multiplying a wind velocity-density spectrum measured at a single point by an "aerodynamic constant." (In the absence of on-site data, a "typical" wind velocity-density spectrum would be used.) If wind-velocity spectra were available for each run, it would be possible to compare them with the corresponding torque-density spectra and thus judge the validity of this method as applicable to this antenna and site and make inference as to its more general validity. This has not yet been accomplished, because the wind data, recorded by pen and ink, are not easily processed in this form. An attempt will possibly be made to carry out this analysis, at least for the runs in which the anemometer was not blanketed by the antenna. Probably a curve tracer will serve to convert the pen-and-ink record to a voltage; this voltage can be recorded and analyzed, using the same equipment which was used to analyze the torque data.

It is recommended that measurements similar to those reported here be conducted on several other large parabolic antennas in order to verify the feasibility of applying these data to different configurations at different sites. Specifically, it is suggested that elevation and azimuth wind-torque measurements be made on one of the similar 60-ft Kennedy antennas at a different site and upon a larger antenna, such as a proposed 150-ft radar antenna. If such work is undertaken, more than one wind-measuring equipment should be used, in order to avoid blanketing by the antenna. The wind speed and direction should be recorded in a fashion favorable to mechanized analysis.

CONCLUSIONS

A limited description has been obtained of the character of the wind torque acting about the elevation axis of a particular 60-ft Kennedy antenna located at the particular site described. Mean-squared torque spectral-density curves have been obtained for 60 different 33-minute runs with a variety of wind conditions and antenna orientations.

*Moll, Kirschbaum, Wetherbee, and Weimer op. cit.

This function may be approximated by the equation:

$$\Phi_{TT} = K \left(\frac{\omega_0^2}{\omega_0^2 + \omega^2} \right) \left(\frac{\omega_1^2}{\omega_1^2 + \omega^2} \right), \quad (16)$$

where

$$K = CV^4$$

$$\omega_0 \simeq 0.12 \text{ rad/sec}$$

$$\omega_1 \simeq 2 \text{ rad/sec}$$

$$V = \text{average wind velocity during run}$$

$$C = \text{a constant of proportionality.}$$

Peak torques were observed during certain runs, and equivalent aerodynamic moment coefficients were derived. The magnitudes of these peak torques show that a very "extreme" wind-velocity profile must have occurred at some time during many of the runs. Root-mean-square values of the variation in the wind-induced torque were obtained for all runs. Similar measurements should be made of the variations in wind-induced torque about the azimuth axis of this antenna or a similar one. Elevation and azimuth torque variations should be measured on several other large antennas to provide further design information.

ACKNOWLEDGMENTS

This project was conceived jointly by the author and Mr. Charles F. White, who also participated in the early planning of the study, and in the interpretation of the data.

Mr. William L. Krewson contributed to the design of the strain-measuring equipment and was the author of Appendix A. Mr. Howard Gordon, Jr. planned the recording system used and supervised the spectrum-analysis procedure. Dr. Ralph O. Belsheim and Mr. John Abel offered useful advice. Most of the data taking and analyses were performed by Mr. Krewson, Mr. David G. Halcombe, and Mr. Philip N. Bradeen.

The antenna was made available by the Radio Communications Branch of the Radio Division.

* * *

APPENDIX A

ANALYSIS OF STRAIN AMPLIFICATION SYSTEM*

The strain-gage mechanical amplifier has been analyzed previously for the case of end deflection of a cantilever beam. It was shown how a specimen of negligible stiffness, clamped between the free end of a cantilever and a fixed point in space, would undergo a strain that was many times greater than the maximum strain found in the beam itself. The amplification ratio for this particular case was, repeating,

$$\frac{\epsilon_1}{\epsilon_2} = \frac{L_1^2}{3cL_2}, \quad (7)$$

where L_1 and L_2 represent the lengths of the cantilever beam and the strain specimen respectively and c is the distance from the neutral axis to the extreme fiber in the cantilever.

Figure A1 is a drawing of the strain amplifier as installed on the antenna. In the actual device, the "fixed structure" of Fig. 8b is replaced with a 6 x 6 in. H-beam (25 lb per ft) bolted to the elevation crank arm of the antenna at one end and connected to this same member at the other end by means of the strain-gage specimen. Consider a wind blowing on the top half of the dish in such a way as to transmit a counterclockwise torque M_0 through the elevation yoke arms to the crank. Here the torque is balanced out by the force F applied at the far end of the crank by the lead screw. Under the action of the force system, the yoke-arm end of the crank rotates through a small angle θ , causing the opposite end of the H-beam to move toward the crank (Fig. A2).

It will be noted that the lead-screw force F has been resolved into two components, with lines of action parallel and normal to the strain specimen. However, only the former component affects the instrumentation readings. The normal force will induce bending in the specimen, but since strain gages are attached to either side, it is possible to cancel out this effect in the bridge network.

If, as shown in Fig. A3, the crank-arm suspension can be approximated by a simply supported beam, with modulus of elasticity E_1 , and if the strain gage specimen can once again be assumed to have negligible stiffness, then the slope θ at the end where the moment is applied equals†

$$\theta = \frac{M_0 L_1}{3E_1 I_1}. \quad (A1)$$

For purposes of simplification, we assume that the crank arm has a constant moment of inertia I_1 along its length.

* By William L. Krewson.

† R. J. Roark, "Formulas for Stress and Strain," p. 102, case 19, New York: McGraw-Hill, 1943.

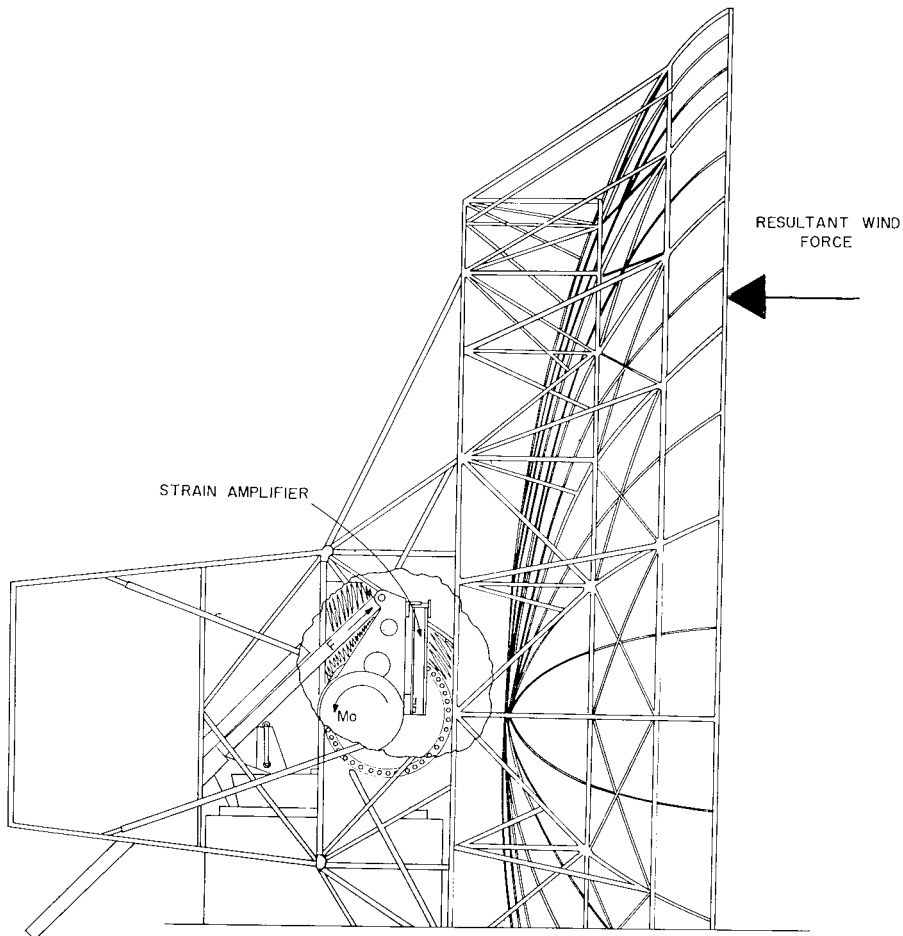


Fig. A1 - Cutaway view of antenna, showing installation of strain amplifier

Fig. A2 - Deflection of crank arm by wind load, H-beam assumed rigid

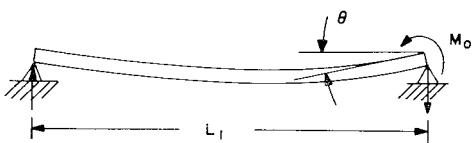
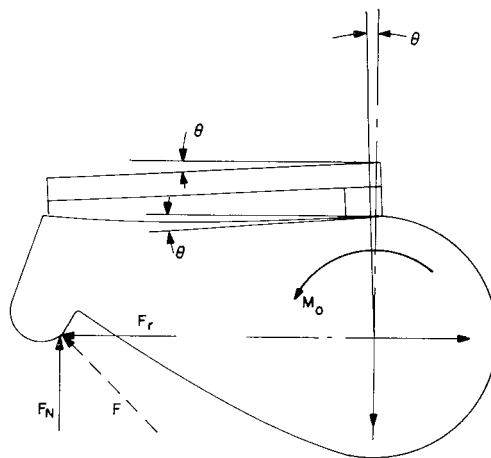


Fig. A3 - Crank arm suspended as a simply supported beam with end couple

Since the strain specimen is presumably unable to restrain the motion of the H-beam, the compression in the gage member, if the H-beam has the same length as the crank, will be

$$\delta_2 = \theta L_1 = \frac{M_o L_1^2}{3E_1 I_1} \quad (\text{A2})$$

which makes the corresponding strain

$$\epsilon_2 = \frac{\delta_2}{L_2} = \frac{M_o L_1^2}{3E_1 I_1 L_2} \quad (\text{A3})$$

The maximum bending moment in the crank arm will equal the applied torque M_o .^{*} Hence the maximum strain ϵ_1 in the crank is[†]

$$\epsilon_1 = \frac{M_o c}{E_1 I_1} \quad (\text{A4})$$

Thus, the strain-amplification ratio, ϵ_2/ϵ_1 , assuming the crank arm simply supported and the strain specimen to have zero stiffness, is

$$\frac{\epsilon_2}{\epsilon_1} = \frac{L_1^2}{3cL_2} \quad (\text{A5})$$

which is identical to Eq. (7), the ratio for the case of the cantilever beam.

Let us now consider the effect of compliance in the H-beam (assumed rigid above) and stiffness in the gage member (previously assumed of zero stiffness) on the last ratio. For this case, the configuration of the strain-amplifier members is as shown in Fig. A4. Once again, the yoke-arm end of the crank has rotated through an angle θ , but because the strain specimen has stiffness of its own, the H-beam no longer assumes the position shown by the dashed line. Instead, the H-beam behaves as a cantilever whose end is deflected upward a distance Δ from the unstrained position. The strain gage compression δ_2 is therefore reduced by the same amount Δ . It now becomes

$$\delta_2 = \theta L_1 - \Delta \quad (\text{A6})$$

If the gage exerts a force P upon the cantilever, the deflection Δ can be stated as

$$\Delta = \frac{PL_1^3}{3E_3 I_3} \quad (\text{A7})$$

where E_3 and I_3 are respectively the modulus of elasticity and the moment of inertia of the H-beam.

^{*}R. J. Roark, "Formulas for Stress and Strain," p.102, case 19; New York:McGraw-Hill, 1943.

[†]The stated crank-arm-strain expression is correct only for the condition shown in Fig. A3. Actually, depending upon the direction of the wind force, compressive or tensile axial loads will also be present at each end of the crank. However, since the cross-sectional area of the crank is sufficiently large and the slenderness ratio (L/r) is relatively small, it seems reasonable to disregard the secondary effect the axial forces will have upon the strain in the crank arm.

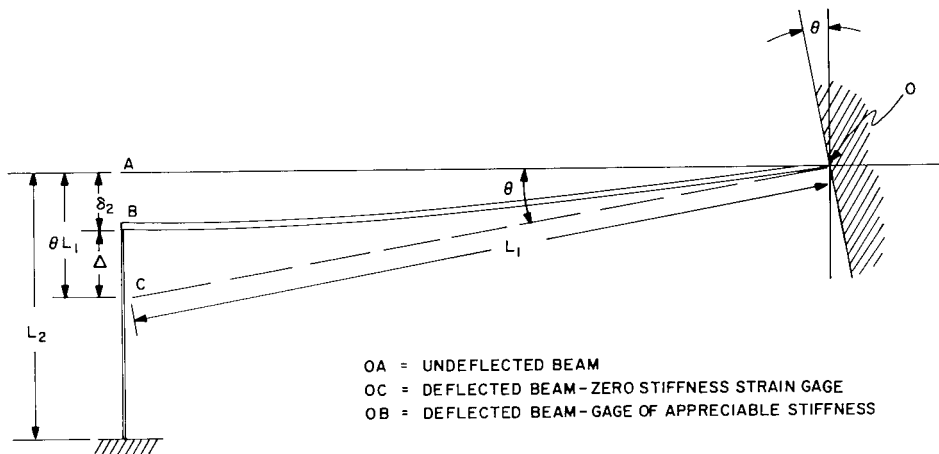


Fig. A4 - H-beam configuration

But P is also the compressive force applied by the cantilever on the strain specimen. Expressed in terms of the gage deflection and the gage modulus of elasticity, cross-sectional area, and overall length (E_2 , A_2 , and I_2), P equals

$$P = \frac{A_2 E_2 \delta_2}{L_2} \quad (A8)$$

Substituting the last two relations and the earlier slope equation, Eq. (A1), into Eq. (A6), and solving for δ_2 , we find

$$\delta_2 = \frac{M_0 E_3 I_3 L_1^2 L_2}{E_1 I_1 (3E_3 I_3 L_2 + E_2 A_2 L_1^3)} \quad (A9)$$

Therefore, the new expression for strain in the gage will be

$$\epsilon_2 = \frac{\delta_2}{L_2} = \frac{M_0 E_3 I_3 L_1^2}{E_1 I_1 (3E_3 I_3 L_2 + E_2 A_2 L_1^3)} \quad (A10)$$

If we divide Eq. (A4), the expression for the maximum strain induced in the crank arm by the applied torque M_0 , into Eq. (A10), we find the new amplification ratio to be

$$\frac{\epsilon_2}{\epsilon_1} = \frac{E_3 I_3 L_1^2}{c (3E_3 I_3 L_2 + E_2 A_2 L_1^3)} \quad (A11)$$

The above ratio can be rearranged to read

$$\frac{\epsilon_2}{\epsilon_1} = \frac{L_1^2}{3cL_2 + \frac{cE_2 A_2 L_1^3}{E_3 I_3}} \quad (A12)$$

Comparing the last expression with Eq. (A5), it is seen that the denominator of Eq. (A12) has been increased by the $cE_2A_2L_1^3/E_3I_3$ term. Thus, the maximum value of strain amplification will result from a flexible gage specimen (small value E_2A_2) and a rigid lever arm (high value E_3I_3). The crank-arm length L_1 and the maximum fiber distance c are, of course, fixed.

Let us assume that the same values for L_1 , L_2 , and c apply as previously. If the strain specimen is made of magnesium with a cross-sectional area of 0.0178 in.², and if the lever arm is a steel H-beam with a moment of inertia of 47 in.⁴, then a closer approximation of the mechanical amplification ratio will be, using the tabulated values below,

$$L_1 = 30 \text{ in.} \quad E_2 = 6.5 \times 10^6 \text{ lbs/in.}^2 \quad I_3 = 47 \text{ in.}^4$$

$$L_2 = 2 \text{ in.} \quad E_3 = 30 \times 10^6 \text{ lbs/in.}^2 \quad A_2 = 0.0178 \text{ in.}^2$$

$$c = 5 \text{ in.}$$

$$\frac{\epsilon_2}{\epsilon_1} = \frac{(30)^2}{(3)(5)(2) + \frac{(5)(6.5 \times 10^6)(0.0178)(30)^3}{(30 \times 10^6)(47)}} = \frac{900}{30 + 11.08} = 21.9.$$

The previous value of the ratio, calculated for a strain gage of negligible stiffness, was $\epsilon_2/\epsilon_1 = 30$.

Since the bending of the actual crank arm cannot be calculated accurately by the simple bending formulas, this answer should be considered as only a rough figure obtained for design purposes. The actual value of ϵ_2/ϵ_1 was obtained implicitly by the calibration procedure.

* * *

APPENDIX B

VALUES OF FIRST CORNER FREQUENCY

As stated in the main body of this report, the values obtained for the first corner frequency, ω_0 , range from 0.03 to 0.29 radians per second. The average of these values is 0.12; the median value is 0.109 radians per second.

The values of ω_0 obtained for most runs are plotted versus average wind speed in Figs. B1 through B6. The runs are grouped, as before, by antenna elevation angle and by azimuth relative to the wind. Seven groups are represented. The other six groups included too few runs to provide a meaningful plot.

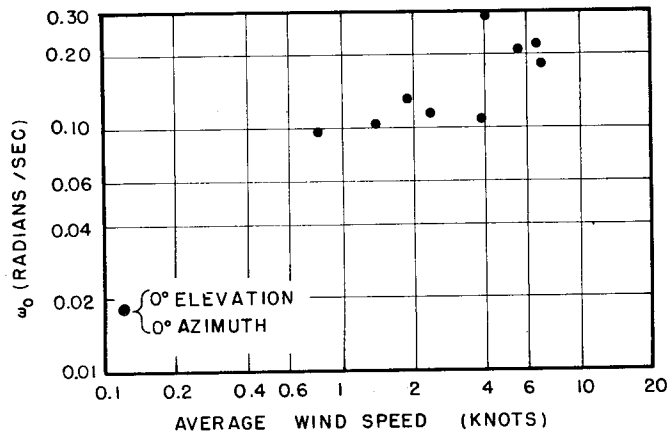


Fig. B1 - Log-log plot of first corner frequency vs average wind speed, 0° elevation, Group I

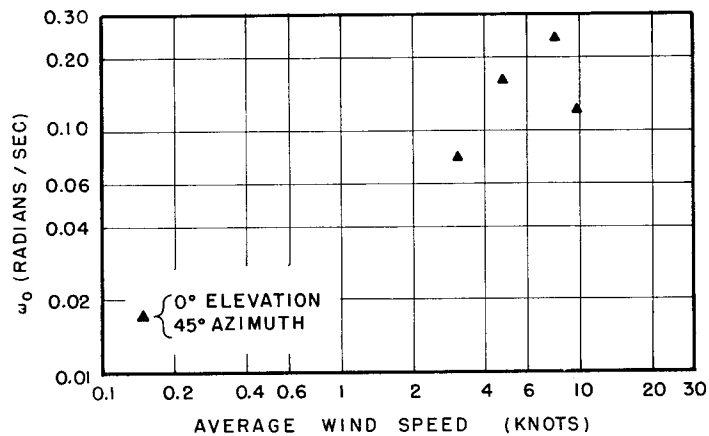


Fig. B2 - Log-log plot of first corner frequency vs average wind speed, 0° elevation, Group II

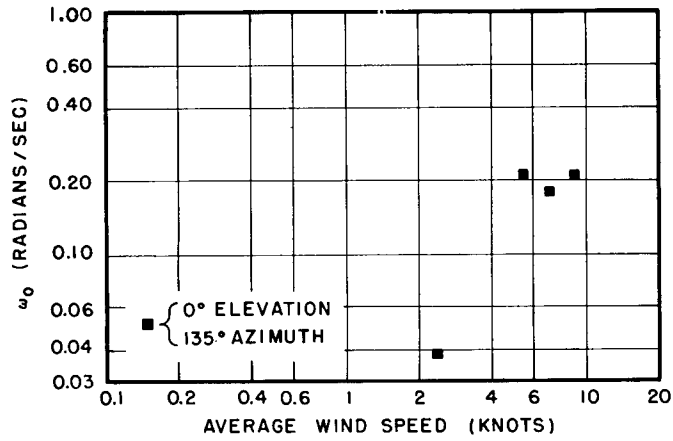


Fig. B3 - Log-log plot of first corner frequency vs average wind speed, 0° elevation, Group IV

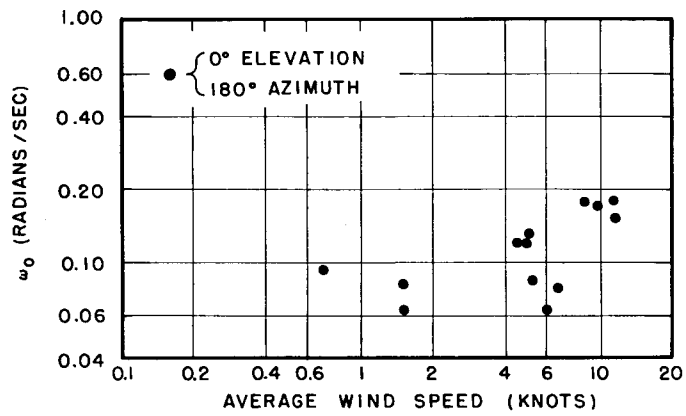


Fig. B4 - Log-log plot of first corner frequency vs average wind speed, 0° elevation, Group V

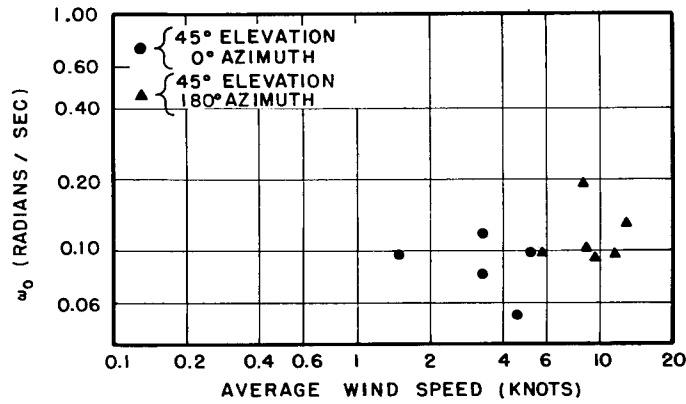


Fig. B5 - Log-log plot of first corner frequency vs average wind speed, 45° elevation, Groups I and V

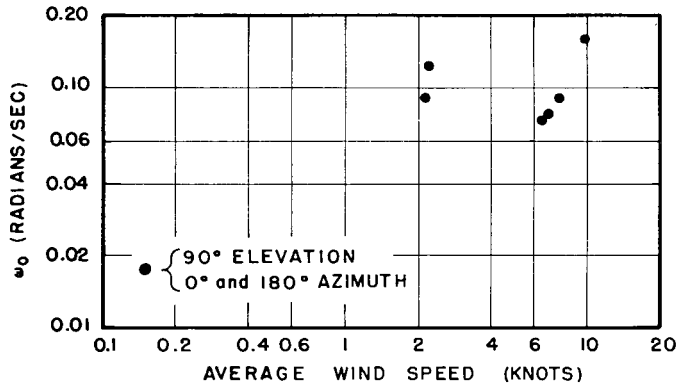


Fig. B6 - Log-log plot of first corner frequency vs average wind speed, 90° elevation, Groups I and V

No attempt was made to represent any of these groups of scattered points by a curve or straight line. These data do not seem to verify the simple physical reasoning which would lead one to expect frequencies to be directly proportional to wind velocity. Selective averaging, however, reveals a slight tendency for higher corner frequencies to be associated with runs made at higher wind velocities, as can be seen from the following list.

Values of First Corner Frequency

- Average of all runs (60) 0.120 radian/sec
- Average of runs with avg. velocity greater than 5.0 kt 0.140 radian/sec
- Average of runs with avg. velocity greater than 6.5 kt 0.143 radian/sec
- Average of runs with avg. velocity greater than 8.0 kt 0.155 radian/sec

* * *

